SPIRou Input Catalogue: Global properties of 440 M dwarfs observed with ESPaDOnS at CFHT

Pascal Fouqué, Claire Moutou, Lison Malo, Eder Martioli, Olivia Lim, Arvind Rajpurohit, Etienne Artigau, Xavier Delfosse, Jean-François Donati, Thierry Forveille, et al.

Monthly Notices of the ROYAL ASTRONOMICAL SOCIETY

MNRAS **475,** 1960–1986 (2018) doi:10.1093/mnras/stx3246
Advance Access publication 2017 December 20

SPIRou Input Catalogue: global properties of 440 M dwarfs observed with ESPaDOnS at CFHT

Pascal Fouqué,[1,2,3]★† Claire Moutou,[1,4] Lison Malo,[1,5] Eder Martioli,[6] Olivia Lim,[1,5] Arvind Rajpurohit,[7] Etienne Artigau,[5] Xavier Delfosse,[8] Jean-François Donati,[2,3] Thierry Forveille,[8] Julien Morin,[9] France Allard,[10] Raphaël Delage,[1] René Doyon,[5] Elodie Hébrard[11] and Vasco Neves[12,13]

[1]*CFHT Corporation, 65-1238 Mamalahoa Hwy, Kamuela, HI 96743, USA*
[2]*Université de Toulouse, UPS-OMP, IRAP, Toulouse, France*
[3]*CNRS, IRAP, 14 avenue Edouard Belin, F-31400 Toulouse, France*
[4]*Aix Marseille Université, CNRS, LAM, Laboratoire d'Astrophysique de Marseille, Marseille, France*
[5]*Institute for Research on Exoplanets, Département de physique, Université de Montréal, CP 6128, Succursale Centre-Ville, Montréal, Quebec H3C 3J7, Canada*
[6]*Laboratorio Nacional de Astrofisica (LNA/MCTI), Rua Estados Unidos, 154, Itajuba, MG, Brazil*
[7]*Astronomy and Astrophysics Division, Physical Research Laboratory, 380009 Ahmedabad, India*
[8]*Université Grenoble Alpes, CNRS, IPAG, F-38000 Grenoble, France*
[9]*LUPM, Université de Montpellier, CNRS, Place Eugène Bataillon, F-34095 Montpellier, France*
[10]*Centre de Recherche Astrophysique de Lyon, UMR 5574, Université de Lyon, ENS de Lyon, Université Lyon 1, CNRS, F-69007, Lyon, France*
[11]*Department of Physics and Astronomy, York University, 4700 Keele St., Toronto, Ontario M3J 1P3 Canada*
[12]*Instituto Federal do Paraná, 85860000, Campus Foz do Iguaçu, Foz do Iguaçu-PR, Brazil*
[13]*Casimiro Montenegro Filho Astronomy Center, Itaipu Technological Park, 85867-900, Foz do Iguaçu-PR, Brazil*

Accepted 2017 December 11. Received 2017 December 7; in original form 2017 November 16

ABSTRACT

Present and future high-precision radial-velocity spectrometers dedicated to the discovery of low-mass planets orbiting low-mass dwarfs need to focus on the best selected stars to make an efficient use of telescope time. In the framework of the preparation of the SPIRou Input Catalogue (SPIC), the CoolSnap program aims at screening M dwarfs in the solar neighbourhood against binarity, rapid rotation, activity, etc. To optimize the selection, this paper describes the methods used to compute effective temperature, metallicity, projected rotation velocity of a large sample of 440 M dwarfs observed in the visible with the high-resolution spectropolarimeter Echelle SpectroPolArimetric Device for the ObservatioN of Stars (ESPaDOnS) at Canada–France–Hawaii Telescope. It also summarizes known and newly discovered spectroscopic binaries, and stars known to belong to visual multiple systems. A calibration of the projected rotation velocity versus measured line widths for M dwarfs observed by the ESPaDOnS spectropolarimeter is derived, and the resulting values are compared to equatorial rotation velocities deduced from rotation periods and radii. A comparison of the derived effective temperatures and metallicities with literature values is also conducted. Finally, the radial-velocity uncertainty of each star in the sample is estimated, to narrow down the selection of stars to be included into the SPIC.

Key words: instrumentation: spectrographs – binaries: general – binaries: spectroscopic – stars: fundamental parameters – stars: low-mass – stars: rotation.

1 INTRODUCTION

Dwarf stars of spectral type M were the coolest stellar objects known until the discovery of field brown dwarfs (Becklin & Zuckerman 1988; Rebolo, Zapatero Osorio & Martín 1995; Nakajima et al. 1995) and the creation of new spectral types L, T, and Y (Martin et al. 1997; Kirkpatrick et al. 1999; Martín et al. 1999; Kirkpatrick 2000). M dwarfs are the most numerous stars in our Galaxy, amounting to about two-thirds in number and about 40 per cent in stellar mass (Kirkpatrick et al. 2012). They were not known from ancient astronomers, as none of them is visible to the naked eye: the brightest one, Gl 825, has a *V* magnitude of 6.7 and

★ E-mail: fouque@cfht.hawaii.edu
† Present address: 65-1238 Mamalahoa Hwy Kamuela, HI 96743, USA.

is an M0V, sometimes classified as K7V. Therefore, M stars were a good example of 'invisible' matter, later recognized as a major contributor to the stellar mass of our Galaxy.

Although they share a common spectral class, they display a wide range in properties: their masses span a range of about a factor 9, similar to the range spanned by B, A, F, G, and K stars altogether. Similarly, their bolometric luminosities span a range of 200. Their global properties vary a lot along the sub-classes from M0 to M9, crossing the limit between stars and brown dwarfs, and as other spectral types, they display a large variety of ages, from pre-main-sequence stars of a few Myr to very old stars, with a corresponding range of radius and therefore gravity for a given mass. They also belong to different star populations (Galactic disc and halo), being classified as dwarfs, subdwarfs, extreme subdwarfs, and even ultra subdwarfs according to their metallicity (Lépine, Rich & Shara 2007).

Lépine & Gaidos (2011) estimate that there are about 11 900 M dwarfs brighter than $J = 10$ in the whole sky. But given their wide range in absolute magnitudes, it is difficult to translate this figure to a given number of M dwarfs within a given distance limit, for instance 25 pc. All the early M dwarfs (up to M3.5V) will then be counted, but not the later spectral type ones. There is no current complete catalogue of late M dwarfs up to a given distance.

In addition, it is well known that M dwarfs display a range of activity, rotational velocity, and magnetic properties (West et al. 2004; Reiners 2007; Kiraga & Stepien 2007; Donati et al. 2008; Morin et al. 2008a,b, 2010, 2011; Irwin et al. 2011; Reiners, Joshi & Goldman 2012; West et al. 2015; Newton et al. 2017 among others), that is further investigated in this study and companion papers (Moutou et al. 2017; Malo et al., in preparation) . Although this class of stars was somehow neglected in the past due to their faintness at optical wavelengths, it started to emerge with the advent of near-infrared sky surveys, DEep Near-Infrared Southern Sky Survey (DENIS) (Epchtein et al. 1999) and Two Micron All Sky Survey (2MASS, Skrutskie et al. 2006), which opened the way to near-infrared spectrometers. As the small mass and radius of M dwarfs were favourable to reveal their planetary companions, and with the additional benefit that their habitable zones lie close enough to the star to allow discoveries of habitable planets, large surveys of these stars began (e.g. Bonfils et al. 2013; Delfosse et al. 2013).

In the framework of the preparation of the new near-infrared high-resolution spectropolarimeter SPIRou (Donati et al., in Deeg & Belmonte (2018)), to be installed at Canada–France–Hawaii Telescope (CFHT) in 2018, members of the SPIRou team decided in 2014 to embark upon an observational snapshot program of M dwarfs, nicknamed CoolSnap, using the ESPaDOnS visible high-resolution spectropolarimeter at CFHT (Donati et al. 1997). The goal of this survey is a better knowledge of M dwarfs selected as prime targets to search for planetary-mass objects in the habitable zone before their inclusion into the SPIRou Input Catalogue (SPIC). The selection criteria used to build the CoolSnap sample are described in Malo et al. (in preparation). Their activity and magnetic properties are described in Moutou et al. (2017). Here, we concentrate on the global properties of the observed stars, such as effective temperature, metallicity, rotational velocity, and binarity. These properties are important for our selection, as we want to avoid stars that are too active, fast-rotating objects, close multiple systems, which will all prevent us from detecting low-mass planets orbiting these stars.

Other near-infrared spectrographs are currently under development, such as Habitable-zone Planet Finder (HPF, Mahadevan et al. 2012), Calar Alto high-Resolution search for M dwarfs with Exoearths with Near-infrared and optical Echelle Spectrographs (CARMENES, Quirrenbach et al. 2014), or GIAno and haRPS (GIARPS, Claudi et al. 2016). These projects can benefit from our study, as we benefited for instance from the CARMENCITA catalogue (CARMENes Cool dwarf Information and daTa Archive, Alonso-Floriano et al. 2015; Cortés-Contreras et al. 2017).

This paper is organized as follows: Section 2 describes how the stars were selected to build a sample of 440 M dwarfs. Section 3 describes spectroscopic binaries either discovered during these observations or already known, and more generally the multiplicity of systems to which stars in our sample belong. Section 4 explains how spectral type, effective temperature and metallicities are derived for our sample, and the limitation of the MCAL method introduced by Neves et al. (2014), and used to measure these properties . Section 5 describes how projected rotation velocities are derived from the width of the Least-Squares Deconvolution (LSD) profile obtained from the observed spectra with an M2 template. Section 6 concludes about stars which are good candidates for radial velocity (RV) search of low-mass planets using the SPIRou near-infrared spectropolarimeter, from the point of view of the parameters measured in this study. Finally, Section 7 summarizes this work and link it to the other two papers in this series, namely Moutou et al. (2017) and Malo et al. (in preparation).

2 SAMPLE AND OBSERVATIONS

We performed our initial compilation of M dwarfs based on the following studies (see Malo et al., in preparation for more details):

(i) An all-sky catalogue of bright M dwarfs (Lépine & Gaidos 2011), which consists of 8889 K7–M4 dwarfs with $J < 10$. This sample is based on the ongoing proper-motion survey using the SUPERBLINK software. Spectral types are estimated from the $V - J$ colour index.

(ii) A catalogue of bright ($K < 9$) M dwarfs (Frith et al. 2013), which consists of 8479 K7–M4 dwarfs. This catalogue rests on the Position and Proper Motion eXtended-L (PPMXL) proper-motion survey.

(iii) An all-sky catalogue of nearby cool stars CONCH–SHELL (Catalogue Of Nearby Cool Host-Stars for Habitable ExopLanets and Life, Gaidos et al. 2014), which consists of 2970 nearby ($d < 50$ pc), bright ($J < 9$) M- or late K-type dwarf stars, 86 per cent of which have been confirmed by spectroscopy. This sample is also selected from the proper-motion survey described in (i), combined with spectra and photometric colour criteria.

(iv) A sample of spectroscopically confirmed nearby M dwarfs (Newton et al. 2014), which consists of 447 M dwarfs with measured metallicities, RVs, and spectral types from moderate resolution ($R \sim 2000$) near-infrared spectroscopy. This sample is drawn from the MEarth survey (Irwin et al. 2011).

(v) A southern sample of M dwarfs within 25 pc (Winters et al. 2015), which consists of 1404 M0–M9.5 dwarfs with $6.7 < V < 21.4$. This sample is based on the REsearch Consortium On Nearby Stars (RECONS) program and supplemented by observations at the Cerro Tololo Inter-american Observatory / Small and Moderate Aperture Research Telescope System Consortium (CTIO/SMARTS) 0.9 m telescope.

(vi) The CARMENES input catalogue of M dwarfs (Alonso-Floriano et al. 2015), which consists of 753 spectroscopically confirmed K–M stars.

(vii) A northern sample of mid-to-late M dwarfs from the MEarth project (Newton et al. 2016), which consists of 387 nearby dwarfs with measured rotation periods.

Table 1. List of four rejected stars.

2MASS name	Common name	Reason for rejection
J07100298−0133146		V=12.196 rather than 13.34 originally used: $V-J=2.23$ therefore corresponds to a K5V–K6V spectral type
J16275072−1926069	TYC 6211−472−1	$J-K_s=1.3$ should have been removed from Gaidos et al. (2014)
J17294104−1748323	TYC 6239−2457−1	wrong PM, not a dwarf; SB1? (us: 3.2 km s^{-1} in 35 d)
J18302580−0006226		$J-K_s=2.0$ should have been removed from Gaidos et al. (2014)
Idem		$V-K_s=7.3$ may be explained by a K giant with circumstellar material: it is an *IRAS* star

This compilation leads to an all-sky sample of about 14 000 K5–M9 stars. Since SPIRou will be installed at CFHT (latitude 20°), we restrict our sample to stars observable with declination north of −30°, which gives a final sample of 10 142 stars.

We applied to this initial sample a merit function computed from the star flux in *H* band and the expected RV amplitude produced by a 3 Earth mass planet orbiting it in the Habitable Zone, which in turn depends upon mass, radius, and temperature of the star, to select the 150 highest merit stars to be observed. Details about this merit function are given in Malo et al. (in preparation).

Observations were conducted with the ESPaDOnS spectropolarimeter (Donati et al. 1997) at the CFHT 3.6 m telescope on top of Maunakea (Hawaii), which provides a wide optical range from 367 to 1050 nm in a single shot at a resolving power of 65 000 (polarimetry) or 68 000 (pure spectroscopy in the so-called star plus sky mode, with one fibre on the target and one on the sky: we call it 'S+S' hereafter). Data are reduced using the LIBRE-ESPRIT software (Donati et al. 1997). LSD (Donati et al. 1997) is then applied to all the observations, to take advantage of the large number of lines in the spectrum and increase the signal-to-noise ratio (S/N per 2.6 km s^{-1} pixel) by a multiplex gain of the order of 10. We used a mask of atomic lines computed with an ATLAS local thermodynamic equilibrium (LTE) model of the stellar atmosphere (Kurucz 1993a). The final mask contains about 4000 moderate to strong atomic lines with a known Landé factor. This set of lines spans a wavelength range from 350 to 1082 nm. The use of atomic lines only for the LSD masks relies on former studies of early and mid-M dwarfs (Donati et al. 2006).

More details about the CoolSnap observations[1] and the data reduction are given in Moutou et al. (2017) and Malo et al. (in preparation). For the purpose of this paper, let us just state that two high S/N spectra (S/N ∼100 at 800 nm) are taken for each M star of the sample (typically M0–M6), separated by several days or weeks, in order to assess possible changes in the magnetic activity or in the heliocentric radial velocity (HRV). We observed 280 spectra in polarimetric mode for 118 stars. Removing four stars initially selected for the CoolSnap sample and observed, but for which classification issues (they most certainly are not M dwarfs) were later discovered, leads to 114 genuine M dwarfs in the CoolSnap sample. The four rejected stars are listed in Table 1 for completeness.

In addition to our own measurements, we searched the ESPaDOnS archive in polarization mode at the Canadian Astronomy Data Center (CADC[2]) from 2005 to 2015 (inclusively) and found 839 spectra for 71 additional M dwarfs (and 10 spectra for two stars in the CoolSnap sample, namely Gl 411 and Gl 905). The two samples have different characteristics, the stars from the archive often being active and rapid rotators and generally having a large number of spectra, while the CoolSnap sample is limited to two spectra taken at different epochs for each star.

Finally, we also searched the ESPaDOnS archives for stars observed in the purely spectroscopic S+S mode. We found 785 spectra for 255 additional stars, raising the total sample of M dwarfs observed with ESPaDOnS to 440.

Spectra of stars belonging to the complementary samples (polarimetric and spectroscopic) have generally been published, but we reanalyse them to derive their effective temperature, metallicity, and projected rotation velocity in a consistent way.

3 MULTIPLE SYSTEMS

Binarity (and higher multiplicity) is common among stars. Many techniques have been devised to disentangle physical association from apparent projection on the sky. A good historical review is given by Dommanget & Nys (2000a). For our purpose, multiplicity may be important for the following reasons:

(i) we may discover that an object initially identified as a single star is in fact a close binary. The selection criterion may then be invalidated when the magnitude or colour encompasses both stars;
(ii) if the components are too close to be separated in the fibre entrance of the spectrograph, both spectra are recorded and the object may then reveal as a single- or double-line spectroscopic binary;
(iii) even when the separation is large enough, and assuming that the system is physical, the planet formation mechanism may have been affected by the binarity;
(iv) wide multiple physical systems composed of an FGK primary and an M secondary allow a calibration of the metallicity of the M dwarf, assuming that it shares the same metallicity as the primary component of the system (see e.g. Bonfils et al. 2005).

The release of originally Global Astrometric Interferometer for Astrophysics (GAIA) data (DR1 and soon DR2) will allow us to confirm the status of the binaries in our sample, and discard the optical systems which are not physical. GAIA will certainly also discover new astrometric binaries in this sample. However, it is still important for future observations to know whether a star has a close

[1] Program IDs 14BF13/B07/C27, 15AF04/B02, 15BB07/C21/F13, 16AF25, 16BC27/F27, and 17AC30, PI: E. Martioli, L. Malo, and P. Fouqué.

[2] http://www.cadc-ccda.hia-iha.nrc-cnrc.gc.ca/en/cfht/

Table 2. Single-line spectroscopic binaries detected in the observations of the CoolSnap sample or listed in the literature and recovered from the ESPaDOnS 'S+S' archive. The HRVs (in $km\,s^{-1}$) and corresponding heliocentric Julian dates (−2450000, at mid-exposure, TT) are given, as measured in our observations.

2MASS name	Common name	SB type	Reference	HRV	HJD	Comment
J00582789−2751251	Gl 46	SB1	This work	23.0, 20.2	7262.029, 7284.933	
J08313744+1923494	GJ 2069B	SB1	Delfosse et al. (1999b)	7.5, 7.5	6813.735, 6814.733	Also in Table A2
J09142298+5241125	Gl 338A	SB1	Cortés-Contreras et al. (2017)	12.3, 11.2	4275.764, 6813.758	Also in Table A2
J10141918+2104297	GJ 2079	SB1?	Shkolnik et al. (2012): table 2	13.0	6771.836	Also in Table A2
J11032125+1337571	LP 491-51	SB1	Cortés-Contreras et al. (2017)	−24.0	4546.875	
J16240913+4821112	Gl 623	SB1	Nidever et al. (2002)	−26.8, −27.2	7226.775, 7402.173	Also in Table A2
J17093153+4340531	GJ 3991	SB1	Reid & Gizis (1997); Delfosse et al. (1999b)	1.0, −54.6	7085.137, 7121.138	
J18495543−0134087		SB1	Malo et al. (2014a)	118.6, 115.3	5747.749, 5747.757	
J22384530−2036519	Gl 867B	SB1	Davison et al. (2014)	4652.100	−2.66	also in Table A2
J22524980+6629578		SB1?	This work	−8.3, −7.6	7611.944, 7680.825	

Table 3. Some special cases of spectroscopic binaries, with discrepant or anomalous results.

2MASS name	Common name	Comment
J03373331+1751145	GJ 3239	SB2, but we measured $v\sin i$ for the primary component (see Table A6).
J08313744+1923494	GJ 2069B	Close VB with an RV drift of $600\,m\,s^{-1}$ over 850 d (Delfosse et al. 1999b), strong magnetic field (Reiners, Basri & Browning 2009).
J10182870−3150029	TWA 6	Non-Gaussian large LSD profile: see Skelly et al. (2008).
J11250052+4319393	LHS 2403	3 low S/N (25) spectra possibly contaminated by the Moon.
J14170294+3142472	GJ 3839	Close visual binary and SB2 (Delfosse et al. 1999b), This work: not clearly SB2, but asymmetrical LSD profile.
J12141654+0037263	GJ 1154	Unresolved SB2 (variable spectral line-width) (Bonfils et al. 2013), strong large-scale magnetic field (Reiners et al. 2009; Morin et al. 2010).
J14493338−2606205	Gl 563.2A	SB2, but we measured $v\sin i$ for the primary component (see Table A6).
J23315208+1956142	Gl 896A	SB1 (Delfosse et al. 1999b), magnetic activity (Morin et al. 2008b).
J23315244+1956138	Gl 896B	SB1 (Delfosse et al. 1999b), magnetic activity (Morin et al. 2008b).

companion, since the light from the companion may contribute significantly to the measured flux, which may affect the measured parameters (magnitudes, colours, etc.).

It is obvious that only a fraction of these systems may affect our observations or the future detection of planetary systems orbiting the stars of our sample. As the fibre diameter is 1.58 arcsec for ESPaDOnS and 1.33 arcsec for SPIRou, binaries separated by less than 1 arcsec will contaminate the observed spectrum. Components separated by more than 2 arcsec should be easy to separate under reasonable seeing. However, at this separation, some parameters may still be affected, such as visual or near-infrared magnitudes.

On another hand, physical separations matter in the rate of formation of planetary systems. Therefore, close physical multiplicity of the stellar system may affect the formation of planets. More details are given in Thebault & Haghighipour (2014).

In order to identify the physical systems (visual or spectroscopic) in our catalogue, we started to build a catalogue of multiple systems involving M dwarfs. We defer to a future publication details and statistics about this catalogue, for instance a confirmation of physical systems based on future released data from GAIA (DR2 and following), and an evaluation of the multiplicity rate among M stars, compared to earlier spectral types, based on a complete distance-limited sample.

3.1 Spectroscopic binaries

Spectroscopic binaries are easily identified when two peaks appear in the LSD profile (SB2). Sometimes, only one component is visible in the spectrum (generally because the other component is much fainter), and we have an SB1. Given that the accuracy of the HRV measured by ESPaDOnS and reduced with LIBRE-ESPRIT (Donati et al. 1997) is about 20–30 $m\,s^{-1}$ (Moutou et al. 2007), SB1 are revealed when the RV corrected to the heliocentric reference frame HRV significantly differs between the two spectra. In Table A1, we list the stars in our sample which have been observed and revealed themselves as SB2 (21 stars including uncertain ones), or even SB3 (2 stars), together with already known spectroscopic binaries (28 SB2, 4 SB3, two quadruple systems SB1+SB2 and SB2+SB2), which should have been excluded when assembling the observational sample.

Among the 57 SB listed in this table, about one half also appears in Table A2, because they belong to multiple systems with both visual and spectroscopic components.

In Table 2, we list the stars in our sample which have been observed and revealed themselves as SB1 (two stars), together with already known single-line spectroscopic binaries (eight stars), also missed when assembling the sample or discovered by others during our survey. RV variations may also be due to activity-induced rotational modulation for stars with strong magnetic fields, rather than binarity. A few special cases with discrepant or anomalous results are listed in Table 3.

3.2 Visual multiple systems detected by imagery

As stated above, it is important to know whether a star in our survey belongs to a physical multiple system. Unfortunately, there is no recent compilation of such systems. Rather than just checking for the multiplicity status of the stars in our sample, we embarked into a

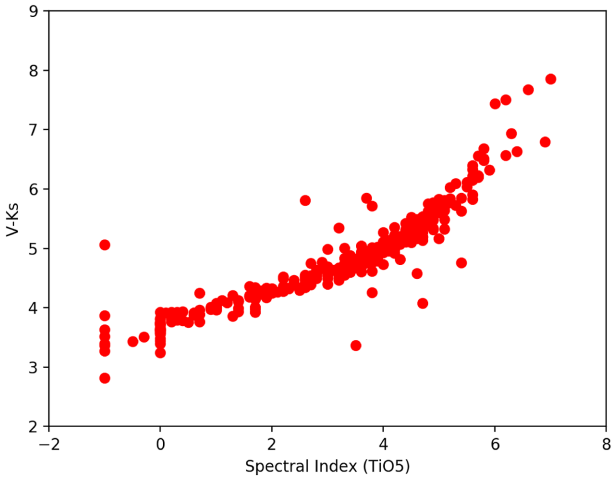

Figure 1. Correlation between the spectral type measured from the TiO_5 spectral index, with the $V - K_s$ colour.

parallel project of listing all multiple systems involving an M dwarf, in order to get better statistics, not biased by the selection process which led to our sample. For this purpose, we surveyed the literature for physical systems detected by imagery, including adaptive optics, coronagraphy, or lucky imaging observations of M dwarfs.

We started by checking the information provided by the Washington Double Star Catalogue (Mason et al. 2001), in its constantly updated online version at CDS (hereafter WDS), the Catalogue of Visual Double Stars observed by the *Hipparcos* satellite (Dommanget & Nys 2000a,b), the Catalog of Physical Multiple Stars (MSC, Tokovinin 1997), the Catalog of Common Proper-Motion Companions (hereafter CPM) to *Hipparcos* stars (Gould & Chanamé 2004), and the Catalogue of Faint Companions to *Hipparcos* stars (Lépine & Bongiorno 2007). We then surveyed the literature for additional binary stars or additional information on the systems described in the above references. Finally, some optical binaries were discovered by us at the telescope, using images from the guider.

The compilation used in this paper is not complete, as we preferred waiting for the second release of GAIA in 2018 April, to discard unphysical multiple systems or components when GAIA measures discrepant parallaxes or proper motions. In its present version, it contains 671 multiple systems, among which 393 have an M dwarf primary. We used this limited version for investigating the multiplicity of stars in our sample of 440 M dwarfs. The resulting table is given in Appendix A.

4 MEASURE OF SPECTRAL TYPE, EFFECTIVE TEMPERATURE, AND METALLICITY

4.1 Spectral type

We estimate the spectral type of our stars from a measurement of the TiO_5 spectral index at 713 nm, as defined and calibrated in Reid, Hawley & Gizis (1995). It is well adapted to the range of spectral types of our sample, at least up to M6.5V. Standard numerical values are adopted, from −1 for K7V, 0 for M0V to 6 for M6V. The correlation with the $V - K_s$ colour is clear, as displayed in Fig. 1. Some stars with an earlier spectral type than our M0 limit (negative spectral indices) or for which we could not measure the spectral type are listed in Table 4. As the limit between spectral classes K7V and M0V is somewhat fuzzy, we prefer not to exclude those stars a priori, without a clear confirmation of a K spectral type. The value of $V - K_s$ may help, as the average value of 25 M0 stars in our sample is 3.65 ± 0.02. Other outliers are generally close visual binaries, where the photometry may be contaminated. They are listed in Table 5.

4.2 The MCAL method

Three important parameters used to characterize stars are effective temperature, metallicity, and gravity. In case of M dwarfs, they are notoriously difficult to measure, especially because no continuum exists in the optical spectrum. There is a long list of publications dealing with several methods to measure mainly the two first, without reaching definite conclusions, for instance Bonfils et al. (2005), Woolf & Wallerstein (2005), Casagrande, Flynn & Bessell (2008), Önehag et al. (2012), Rojas-Ayala et al. (2012), and Rajpurohit et al. (2013).

In this work, we chose to use the MCAL method of measurement described in Neves et al. (2014). In short, it is based on measurements of pseudo-equivalent widths of lines in high-resolution optical spectra obtained by Bonfils et al. (2013) using the High Accuracy Radial velocity Planet Searcher (HARPS) spectrometer, which are then correlated to known values of $T_{\rm eff}$ and [Fe/H] from Casagrande et al. (2008) and Neves et al. (2012), respectively. A caveat is that gravity is not used in this correlation, so young stars with low gravity probably get assigned a biased temperature and metallicity.

For this study, we started by using the Neves et al. (2014) calibration: the calibrating $T_{\rm eff}$ values come from Casagrande et al. (2008) $T_{\rm eff}$ versus colour relations. The authors enhanced the infrared flux method (Blackwell et al. 1990), to apply it to M dwarfs by adding information from the optical range. Their new method is called MOITE (Multiple Optical-Infrared TEchnique). In this method, the bolometric flux comes from optical and infrared photometry for about 80 per cent, and the rest comes from Phoenix models[3] described for instance in Hauschildt et al. (1999).

Although this method allows one to derive metallicities, Neves et al. (2014) prefer to use their own metallicity values. These are based on a technique pioneered by Bonfils et al. (2005). It starts with binary stars where the primary component is a star of spectral type F, G, or K which has a spectroscopically measured metallicity, and the secondary is an M dwarf assumed to share the metallicity of the primary. These binary M dwarfs serve in turn to calibrate an M_k versus $V - K_s$ colour–magnitude diagram: the main-sequence locus at an average metallicity is identified, and the colour or absolute magnitude shift from this locus gives a measure of the metallicity of new M stars. Subsequently, Johnson & Apps (2009) corrected the calibration for metal-rich M stars, and Schlaufman & Laughlin (2010) refined that latter calibration. Mann et al. (2013a) compiled and measured metallicities of solar-type primaries in 112 wide binary systems involving an M dwarf secondary. Maldonado et al. (2015) used a similar method to MCAL to calibrate stellar parameters of 53 M dwarfs observed with HARPS.

Neves et al. (2012) refined once more over Schlaufman & Laughlin (2010). Using this calibration, Neves et al. (2013) computed the metallicity of all the M dwarfs in the Bonfils et al. (2013) sample and Neves et al. (2014) selected the more suitable for their calibration of the pseudo-equivalent widths versus metallicity and effective temperatures. Their table 2 contains 65 stars, and the calibrating values are given in the columns labelled [Fe/H]_N12 and

[3] ftp.hs.uni-hamburg.de/pub/outgoing/phoenix/GAIA/

Table 4. List of 13 stars with undetermined or negative spectral types.

2MASS name	Common name	Spectral type (TiO_5)	Spectral type	$V-K_s$	Possible explanation
J00161455+1951385	GJ 1006A	−1.0	M4V	5.058	
J00233468+2014282	FK Psc	−0.3	K7.5V	3.505	
J00340843+2523498	V493 And	−0.5	M0V	3.436	
J01373940+1835332	TYC 1208-468-1	−1.0	K3V+K5V	3.868	
J02272804+3058405	BD+30 397B	−1.0	M2V		Young M dwarf in βPic (Shkolnik, Liu & Reid 2009)
J02272924+3058246	AG Tri	None	K7V	3.205	Young M dwarf in βPic (Shkolnik et al. 2009)
J08081317+2106182	LHS 5133	−1.0	K7V	3.392	
J10112218+4927153	Gl 380	−1.0	K7V	3.636	
J11220530−2446393	TWA 4	−1.0	K5V	3.519	
J12245243−1814303	Gl 465	None	M3V	4.300	Large rotation ($v\sin i = 63\,\mathrm{km\,s^{-1}}$)
J16575357+4722016	Gl 649.1B	None	M1.5Ve		maybe Gl 649.1A (K3V) at 5.1" was observed
J20560274−1710538	TYC 6349-200-1	−1.0		3.370	
J22465311−0707272		−1.0		2.822	Photometry may be contaminated by a star at 4.3"

Table 5. Stars with discrepant $V-K_s$ colours for their spectral index.

2MASS name	Common name	Spectral type (TiO_5)	$V-K_s$	Comment
J01034013+4051288	NLTT 3478	3.5	3.370	Visual binary 0.3 arcsec
J01034210+4051158	NLTT 3481	4.6	4.584	Visual binary 2.5 arcsec
J01591260+0331113	NLTT 6638	3.2	5.351	SB2 and visual binary
J08313744+1923494	GJ 2069B	4.7	4.081	Visual binary 1.0 arcsec
J08524466+2230523	NLTT 20426	3.8	4.260	Visual binary 4.6 arcsec
J11314655−4102473	Gl 431	3.8	5.719	
J17462507+2743014	Gl 695BC	3.7	5.847	Visual binary 0.8 arcsec
J18450905−0926438	TYC 5696-202-2	2.6	5.815	
J22171870−0848186	Gl 852B	5.4	4.759	Visual binary 1.0 arcsec

Teff_C08. It should be noted that some of these values differ from the similar previous table A.1 in Neves et al. (2013), probably because of a change in the adopted V magnitude of the star, which in turn produces a change in the distance to the main-sequence locus and therefore of its computed $T_{\rm eff}$ from colours.

4.3 Limits of the method

Not all spectra are usable when applying the MCAL method. Some spectra have low S/N, giving an ill-defined peak in the LSD profile, or an inaccurate RV. Two stars (vB8 and vB10) have nine spectra each in the Polar archive (published in Morin et al. (2010), with S/N between 68 and 107, but they have very late spectral types (M7V and M8V, respectively) outside of the calibration range of the method. In polarimetric mode, we are therefore working on 1090 spectra taken with a large enough S/N (typically, S/N per $2.6\,\mathrm{km\,s^{-1}}$ pixel >100), for 182 stars, removing the two very-late dwarfs mentioned above and 2MASS J09002359+215054, which only has one spectrum with an S/N of 30 in the CoolSnap sample. Similarly, some S+S spectra have a low S/N which does not meet our original quality criterion for polarimetry (S/N >100). We only exploited S+S spectra of good quality (well-detected LSD profile, correct RV), reducing the number of useful spectra to 706 for 298 stars (including 45 with polarimetric spectra too), which added to the 182 stars with useful polarimetric spectra leads to a total of 435 stars which can a priori be used to measure global parameters.

But in fact, as explained by Neves et al. (2014), some very active stars are not suitable to the measurement of $T_{\rm eff}$ and [Fe/H] by this method. As many stars in the ESPaDOnS archive are active, this can drastically reduce the sample of stars where those parameters can be measured. To identify very active stars, the method measures an Hα index as defined in Gomes da Silva et al. (2011). A small value of about 0.03 corresponds to inactive stars. The adopted cut-off is a value of 0.25, roughly corresponding to a luminosity ratio $\log L_{\rm H\alpha}/L_{\rm bol}$ of −4.0, above which $H\alpha$ and magnetic flux become independent of the rotation rate, as shown in Reiners et al. (2009). According to this cut-off between saturated (or very active) and non-saturated stars, our CoolSnap sample contains 10/113, the polarimetric archive 40/69, and the spectroscopy archive 146/253 very active stars, for which metallicity and effective temperatures cannot be reliably measured by the MCAL method. An additional 33 non-saturated stars are spectroscopic binaries, for which the method does not work properly either (see above). Finally, a few non-saturated rapid rotators are not well suited either to this technique, as the measurement of pseudo-equivalent widths is affected by the broadening of the lines due to rotation, and the calibration therefore returns too low temperatures. We do not consider measured effective temperatures and metallicities for 20 non-saturated stars with a $v\sin i$ larger than $8\,\mathrm{km\,s^{-1}}$. We are left with 192 stars on which comparisons with other methods can be secured.

The main source of accurate $T_{\rm eff}$ comes from the work of Boyajian et al. (2012), who measure M dwarf radii using the Center for High Angular Resolution Astronomy (CHARA) interferometer. They then compute the bolometric flux from multiband photometry and derive a value of $T_{\rm eff}$. This seems to be a straightforward method, if the template spectra fitted to the photometry are reliable. Mann, Gaidos & Ansdell (2013b) argue that when compared to their actual low-resolution spectra, there are systematic differences, leading to underestimated bolometric fluxes and temperatures. Finally, Mann et al. (2015) use the same method to measure the bolometric flux, but use the Cosmological Impact of the First STars (CIFIST) team suite of the BT-Settl version of the PHOENIX atmosphere models (Allard et al. 2013), to measure $T_{\rm eff}$ and derive the corresponding radii.

Both Mann et al. (2015) and Rajpurohit et al. (2013), who measured $T_{\rm eff}$ by fitting BT-Settl synthetic spectra, show that $T_{\rm eff}$ values from Casagrande et al. (2008) are too low due to the assumption that M dwarf can be treated as black bodies beyond 2 µm. As the Casagrande et al. (2008) temperature scale is used in the original MCAL method used by Neves et al. (2014), it is important to confirm this result. For this purpose, we compared the original Neves et al. (2014) calibration to other sources of measurements, for instance Woolf & Wallerstein (2005, 2006), who use CaH_2 and TiO_5 molecular band strength indices, Önehag et al. (2012), Lindgren, Heiter & Seifahrt (2016), and Lindgren & Heiter (2017), who fit synthetic spectra to high-resolution Very Large Telescope / CRyogenic high-resolution InfraRed Echelle Spectrograph (VLT-CRIRES) spectra in the *J* band, which are free from large molecular-band contributions, or Rojas-Ayala et al. (2012), who measure equivalent widths of CaI and NaI lines in the near-infrared and a spectral index quantifying the absorption due to H_2O opacity. We found a faire agreement for the metallicities (within 0.2 dex), but the effective temperatures obtained using the original calibration are systematically low by about 200 K.

We therefore adopt the Mann et al. (2015) $T_{\rm eff}$ scale while retaining the Neves et al. (2014) metallicity scale. We modified the original MCAL code to recompute the coefficients of the calibration relations using the more recent and accurate source of $T_{\rm eff}$. The code contained a revised table of 68 calibrators, adding three stars to Neves et al. (2014, Table 2: Gl 388, Gl 551, and Gl 729). Among these calibrators, only 29 have $T_{\rm eff}$ and [Fe/H] values in Mann et al. (2015). We therefore use these 29 stars with Mann et al. (2015) $T_{\rm eff}$ (ranging from 3056 to 3848 K) and Neves et al. (2014) [Fe/H] (ranging from −0.51 to 0.19 dex) to recalibrate the matrices given in Neves et al. (2014). The median differences between Mann et al. (2015)- and Neves et al. (2014)-based calibrations are: $\Delta T_{\rm eff} = 180 \pm 80$ K and Δ[Fe/H] $= 0.04 \pm 0.12$ dex. Similarly, median differences between the Mann et al. (2015)-based calibration and Rojas-Ayala et al. (2012) for 21 stars in common are: $\Delta T_{\rm eff} = 240 \pm 170$ K and Δ[Fe/H] $= 0.08 \pm 0.11$ dex. This confirms the offset of about 200 K in temperature and the fair agreement in metallicity.

The list of stars used in this comparison is given in Table A3 in Appendix A. Spectroscopic binaries have been removed from this comparison: SB2 have double lines which probably affect the determination of the continuum, and there is a risk to mix both components in the measurements of the lines. SB1 are a priori more immune, but the secondary may affect the line depth, which is used in the determination of both effective temperature and metallicity in the MCAL method.

Promising new techniques to derive effective temperature, metallicity, and gravity of M dwarfs have been pioneered by Rajpurohit et al. (2013), using high-resolution stellar spectra and up-to-date model atmospheres. They look for the best combination of the three parameters used as an input to generate BT-Settl synthetic spectra which reproduce the observed spectra. We are in the process of applying this method described in Rajpurohit et al. (2017) to our spectra. Unfortunately, preliminary results show a good agreement only for effective temperatures, but no correlation for metallicities. An example of fitted spectrum is given in Fig. 2. A more thorough comparison of our results with BT-Settl synthetic spectra will be deferred to a future paper.

Finally, a similar comparison using specific wavelength windows in which line parameters were corrected to provide an optimal fit to some standard stars with known parameters is also in progress (Kulenthirarajah et al., in preparation).

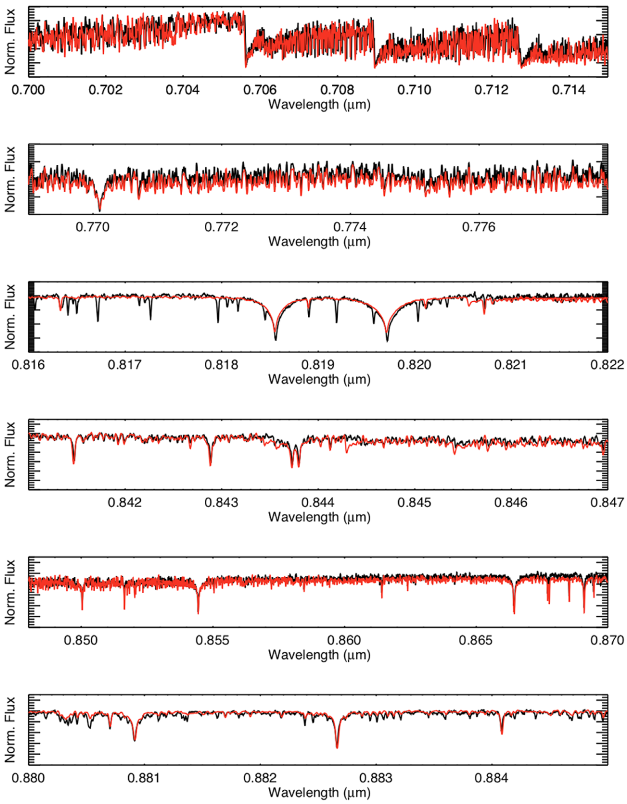

Figure 2. Comparison of an observed ESPaDOnS spectrum (in black) with the corresponding synthetic spectrum (in red) from a BT-Settl model for $T_{\rm eff} = 3300$ K, [Fe/H]=−0.10 dex, and $\log g = 5.0$ between 700 and 885 nm.

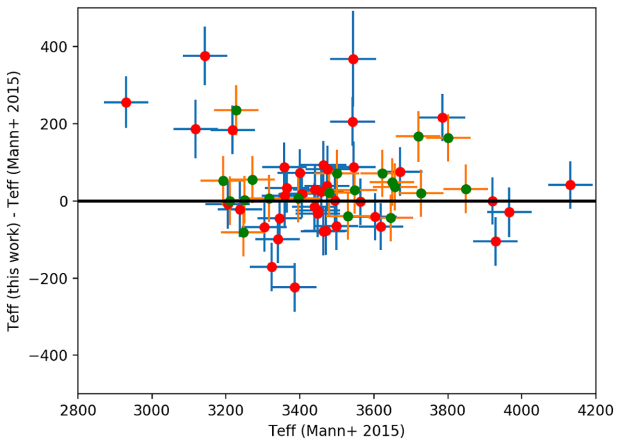

Figure 3. Difference between our effective temperatures and reference values from Mann et al. (2015). Green points (with orange error bars) correspond to stars used in the recalibration of the MCAL method, and red points (with blue error bars) to additional stars.

4.4 Comparison of results

Fig. 3 shows a comparison of our effective temperatures to corresponding values from Mann et al. (2015). We adopt their uncertainty on $T_{\rm eff}$ as listed (typically 60 K) and a quadratic sum of the uncertainty returned by MCAL and a systematic uncertainty of 60 K for our measurements, based on the observed dispersion between the two sets. The agreement is not surprising as our recalibration of MCAL method is based on 29 effective temperatures from Mann et al. (2015, green points), but we have more measured stars

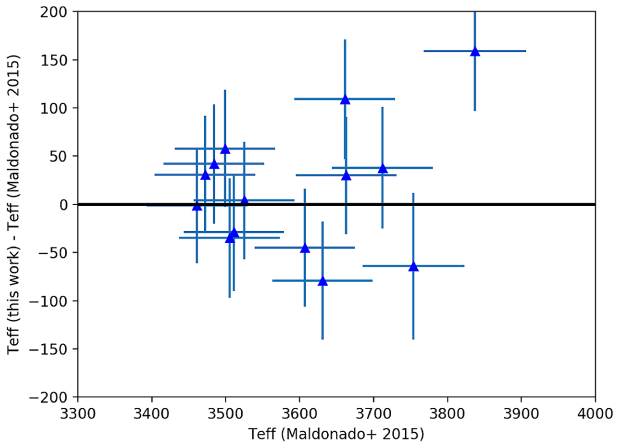

Figure 4. Difference between our effective temperatures and values from Maldonado et al. (2015).

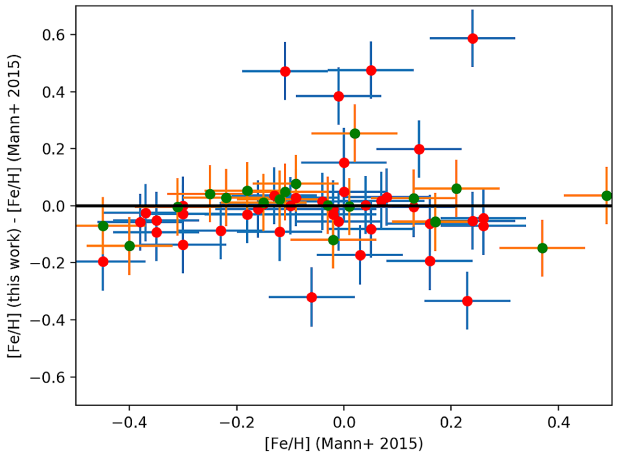

Figure 5. Difference between our metallicities and reference values from Mann et al. (2015). Green points (with orange error bars) correspond to stars used in the re-calibration of the MCAL method, and red points (with blue error bars) to additional stars.

(red points) and not all 29 calibrators have an ESPaDOnS spectrum. After rejecting three outliers from the sample (LHS 1723, Gl 297.2B, and HH And=Gl 905), the mean difference between the two systems computed from 57 stars is $T_{\rm eff}$ (this work) – $T_{\rm eff}$ (reference) = 20 ± 12 K with an rms of 90 K. Given that Mann's temperatures have a typical uncertainty of 60 K, it shows that our effective temperatures should have a similar accuracy, and we therefore adopt a systematic uncertainty of 60 K for our measurements.

We also compare our results to the work of Maldonado et al. (2015), who use a similar method to MCAL to estimate effective temperatures and metallicities. We adopt their uncertainty on $T_{\rm eff}$ as listed (typically 68 K) and a quadratic sum of the uncertainty returned by MCAL and a systematic uncertainty of 60 K for our measurements. Unfortunately, their sample is limited to early-type stars, but the agreement with our effective temperatures is also satisfactory, as can be seen in Fig. 4 (mean difference, this work minus Maldonado et al. 2015: +16 ± 17 K, σ = 64 K).

For the metallicity comparison, Fig. 5 displays the results from Mann et al. (2015) compared to ours. We adopt an uncertainty on the [Fe/H] values from their paper (typically 0.08 dex), and a quadratic sum of the uncertainty returned by MCAL and a systematic uncertainty of 0.10 dex, based on the observed dispersion between

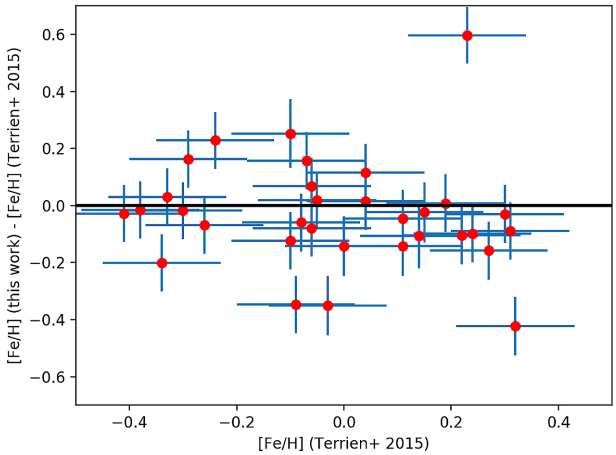

Figure 6. Difference between our metallicities and values from Terrien et al. (2015).

the two sets. This is a more meaningful comparison than for effective temperatures, as Mann's metallicities have not been used in our recalibration. It shows a generally good agreement, but some of our metallicities seem too high. These correspond to K7V–M0V stars, which have effective temperatures slightly out of our calibration domain. Rejecting the same three stars, the mean difference between the two systems is [Fe/H] (this work) – [Fe/H] (reference) = 0.014 ± 0.020 dex with an rms of 0.15 dex. Given that Mann et al. (2015) claim an accuracy of 0.08 dex, our accuracy would be about 0.13 dex. However, removing four K7V–M0V stars with discrepant metallicities still gives a negligible offset of −0.021 ± 0.011 dex, but with an rms of 0.08 dex. We therefore adopt a systematic uncertainty of 0.10 dex for our values of [Fe/H] when the effective temperatures fall within the limits of our calibration (3056–3848 K), to be added quadratically to the generally negligible uncertainty returned by MCAL.

A more independent comparison for metallicities has been made with the results obtained by Terrien et al. (2012), who measure equivalent widths of Na, Ca, and K lines in the near-infrared (*H* and *K* bands), and correct for effective temperature effects using H_2O indices. Thirty-three non-active stars were found in common with Terrien et al. (2015), and the comparison is displayed in Fig. 6. We adopt a uniform uncertainty of 0.11 dex on the [Fe/H] values from Terrien et al. (2015), as stated in their paper, and a quadratic sum of the uncertainty returned by MCAL and a systematic uncertainty of 0.10 dex. The agreement is satisfactory (mean difference, this work minus Terrien et al. 2015: −0.055 ± 0.026 dex, σ = 0.15 dex).

5 MEASURE OF THE PROJECTED ROTATION VELOCITY

In order to measure the rotation of these stars from our polarimetric observations, we need a calibration of the rotational velocity of M dwarfs from the observed width of the LSD profile given by the LSD technique, described in Donati et al. (1997).

We use M dwarfs of known $v \sin i$ from the literature for which high-resolution spectra have been obtained with ESPaDOnS, most of them from archival data and some from the CoolSnap program itself. We have combined both polarimetric and S+S spectra, assuming that the spectral resolution is the same (in fact 65 000 versus 68 000).

5.1 Sample and measurement techniques

We based our compilation of $v\sin i$ values from the literature on the catalogue of 334 M dwarfs in Reiners et al. (2012). We only retained stars with a measured value of $v\sin i$, not those with an upper limit. We then added a few stars from Reiners & Basri (2007), Donati et al. (2008), Morin et al. (2008b), Reiners et al. (2009), and Morin et al. (2010) which were missing from the 2012 compilation. Very recently, Reiners et al. (2017) published a spectroscopic survey of 324 M dwarfs, where resolved values of $v\sin i$ are listed for 78 stars. This allowed us to revise old values of $v\sin i$ and add new calibrators.

Cross-matching the 440 M dwarfs observed with ESPaDOnS in our sample with the list of $v\sin i$ calibrators, we end up with 62 common stars with $v\sin i$ values ranging from 1.0 to 55.5 km s^{-1}. Removing two stars which are SB2 (Gl 268 and Gl 735) gives 60 calibrators listed in Table 6.

To calibrate our $v\sin i$ measurements, we used three approaches: a first approach uses a calibration of $v\sin i$ versus the observed width of the LSD profile, taking into account an intrinsic width which depends on the spectral type of the star. This is the approach adopted by Delfosse et al. (1998) for the ELODIE fiber-fed echelle spectrograph at Observatoire de Haute-Provence (OHP), Melo, Pasquini & De Medeiros (2001) for the Fiber-fed Extended Range Optical Spectrograph (FEROS) spectrograph, Boisse et al. (2010) for Spectrographe pour l'Observation des PHenomenes des Interieurs stellaires et des Exoplanetes (SOPHIE) at OHP, Houdebine & Mullan (2015), both for SOPHIE and HARPS at European Southern Observatory, La Silla. We find that the intrinsic width, defined as the lower envelope of the observed width, slightly depends on the spectral type. However, it has to be recalled that we use a single template spectrum (mask) for all the stars that we correlate with the observed spectrum. So any mismatch between the actual spectral type of the star and the spectral type of the mask (M2) translates into a modification of the LSD profile.

A second approach uses an FeH line at 995.0334 nm to better estimate the intrinsic broadening of the line due to rotation. This line is insensitive to gravity and magnetic field (Reiners 2007) and should give a more direct comparison among stars of different spectral types than the LSD profiles. The measurement quality, however, is worse than when thousands of lines are used.

Finally, a third approach uses a few slow rotators for which the value of $v\sin i$ is known from the literature, and a high S/N polarimetric spectrum taken with ESPaDOnS exists. By broadening the LSD profile of a calibrator using different values of $v\sin i$ and comparing to the observed spectrum of a given star, we can then select the best calibrator and deduce the best value of $v\sin i$ reproducing the observed spectrum. This assumes that rotation is the main contributor to the width of the LSD profile, which means that we assume that convective turbulence and magnetic field broadening can be neglected. All methods better work for stars where the projected rotational velocity has a significant impact on the global line broadening.

5.2 First approach: measure of the LSD profile

The LSD software (Donati et al. 1997) uses a line list built from an ATLAS9 LTE model (Kurucz 1993a,b) matching the properties of M2 stars, which contains about 5000 atomic lines weighed by their intensity. The multiplex gain is about 10 in S/N.

5.2.1 *Variation of $\sigma_\circ$ with spectral type*

A necessary step in the calibration of $v\sin i$ from the width of the LSD profile is to estimate at each spectral type the minimum value of the width which can be measured. We measure the width of the LSD profile by fitting a Gaussian profile and measuring the value of σ, and we use the $V-K_s$ colour as a quantitative estimate of the spectral type of the stars in our sample. We reject spectra with an S/N lower than 30. A diagram of σ versus $V-K_s$ is displayed on Fig. 7 and clearly shows an accumulation of points at small values of σ. The minimum value of σ could be measured as the mode of the distribution in colour bins. In practice, we fit a lower envelope by eye, and it can be seen that it fits both polarimetric measurements (black points) and S+S spectra (orange points). The minimum value of this lower envelope is about 4 km s^{-1}, corresponding to a full width at half-maximum of the LSD profile of 9 km s^{-1}. It is obtained at a $V-K_s$ of about 5, corresponding roughly to an M4 spectral type. For earlier- or later-spectral types, the minimum values are higher.

Equation (1) describes the variation of $\sigma_\circ$ with the $V-Ks$ colour for the LSD profile:

$$3\sigma_\circ = 11.39 - 3.06\,(V-Ks) + 0.308\,(V-Ks)^2 \pm 0.32 \pm 0.12 \pm 0.011. \quad (1)$$

5.2.2 *Calibration of* v*sin* i *versus* σ

Once we have an estimate of the intrinsic width $\sigma_\circ$ at a given colour or spectral type, we need to subtract it quadratically from the measured width to get a measurement of the rotational broadening. As the intrinsic width is given by the lower envelope fitting the mode of the widths distribution, we are unable to measure the projected rotation velocity of slow rotators having a measured width similar or even smaller than the intrinsic width, due to measurement uncertainties. We discard these rotators in the calibration of $v\sin i$ versus rotational broadening, and adopt an upper limit of 2 km s^{-1} for their value of $v\sin i$. In summary, we define the rotational broadening as Δ, given by equation (2):

$$\Delta = \sqrt{\sigma^2 - \sigma_\circ^2}. \quad (2)$$

Table 6 gives a list of the 60 stars used to calibrate these relations. Stars with an * have not been used in the calibration of the FeH relation (see below). When an uncertainty is not given in the reference of $v\sin i$, we adopt 10 per cent of $v\sin i$, with a minimum value of 1.5 km s^{-1}.

We then plot the literature measurements of $v\sin i$ versus Δ in Fig. 8. The largest rotator (GJ 3789 at $v\sin i = 55.5$ km s^{-1}) does not fit well the trend and is then rejected in order not to bias the calibration. Gl 412B is a clear outlier (strong magnetic slow rotator) and is removed too before the fit. Finally, we could not measure the value of σ for three stars because their spectra have an S/N smaller than 30, and one star has a σ value slightly smaller than the adopted $\sigma_\circ$ for its colour.

The functional shape of the fitting curve is not exactly linear: at large values of Δ we want $v\sin i$ proportional to Δ and at small values of Δ we want small $v\sin i$. We adopt the following function:

$$v\sin i = \Delta\,\frac{a\,\Delta + b}{\Delta + c}. \quad (3)$$

Resulting values of a, b, and c in equation (3) over 54 calibrators are:

$$a = 1.75 \pm 0.06,$$
$$b = 2.10 \pm 0.68,$$
$$c = 5.41 \pm 0.63.$$

This gives a reasonable fit valid up to about 40 km s^{-1}, displayed in Fig. 8.

Table 6. List of stars with known $v\sin i$ used to calibrate equation (3) (all stars) and equation (5) (except stars with *).

2MASS name	Common name	$V-K_s$	$\sigma_\circ$	$\langle\sigma\rangle$	$\sqrt{\langle\sigma\rangle^2-\sigma_\circ^2}$	Literature $v\sin i$	Original error	Reference
J01023895+6220422	Gl 49	4.194	3.97	4.22	1.43	1		Donati et al. (2008)
J01031971+6221557	Gl 51	5.635	3.92	11.24	10.53	12.0		Morin et al. (2010)
J01592349+5831162	Gl 82	5.194	3.80	10.57	9.86	13.8		Reiners et al. (2012)
J02085359+4926565	GJ 3136	4.867	3.79	16.73	16.29	24.1	2.4	Reiners et al. (2017)
J02333717+2455392	Gl 102	5.351	3.83	5.74	4.27	3.0	1.5	Reiners et al. (2017)
J02515408+2227299		5.208	3.80	17.68	17.26	27.2	2.7	Reiners et al. (2017)
J03462011+2612560	HD 23453	3.799	4.21	4.52	1.64	3.3	4.0	Reiners et al. (2017)
J03472333−0158195	G 80-21	4.626	3.82	6.87	5.71	5.2	1.5	Reiners et al. (2017)
J04374092+5253372	Gl 172	3.601	4.36	4.65	1.62	3.4	1.5	Reiners et al. (2017)
J04593483+0147007	Gl 182	3.807	4.20	7.86	6.65	10.4		Reiners et al. (2012)
J05082729−2101444		5.832	4.02	23.43	23.09	25.2	2.5	Reiners et al. (2017)
J05312734−0340356	Gl 205	3.866	4.16	4.29	1.06	1.5		Reiners (2007)
J05363099+1119401	Gl 208	3.669	4.30	4.88	2.31	3.8	1.5	Reiners et al. (2017)
J06000351+0242236	GJ 3379	5.274	3.81	6.62	5.41	4.9	1.5	Reiners et al. (2017)
J06103462−2151521	Gl 229	4.016	4.06	4.23	1.19	1.0		Reiners (2007)
J07444018+0333089	Gl 285	5.321	3.82	7.71	6.70	4.0	1.5	Reiners et al. (2017)
J08115757+0846220	Gl 299	5.169	3.80	5.13	3.45	3.0	1.7	Delfosse et al. (1998)
J08294949+2646348	GJ 1111	7.680	6.06	10.37	8.42	10.5	1.5	Reiners et al. (2017)
J08313744+1923494	GJ 2069B	4.081	4.03	8.26	7.21	6.5	1.7	Delfosse et al. (1998)
J09002359+2150054	LHS 2090	7.503	5.77			14.3	1.5	Reiners et al. (2017)
J09142485+5241118	Gl 338B	3.584	4.38	4.41	0.52	2.3	1.5	Reiners et al. (2017)
J09445422−1220544	G 161-71	6.149	4.22	23.67	23.29	31.2	3.1	Reiners et al. (2017)
J10121768−0344441	Gl 382*	4.250	3.94	4.13	1.23	1.8		Reiners (2007)
J10193634+1952122	Gl 388	4.871	3.79	6.00	4.65	3.0		Reiners (2007)
J10285555+0050275	Gl 393	4.276	3.93	4.14	1.28	1.5		Reiners (2007)
J10481258−1120082	GJ 3622	7.858	6.36	7.61	4.17	2.1	1.5	Reiners et al. (2017)
J10562886+0700527	Gl 406	7.444	5.68	7.26	4.53	3.0		Reiners & Basri (2007)
J11023832+2158017	Gl 410	3.884	4.15	4.77	2.36	2.6	1.5	Reiners et al. (2017)
J11053133+4331170	Gl 412B*	6.611	4.62	15.78	15.09	8.2	2.7	Reiners et al. (2017)
J11314655−4102473	Gl 431	4.986	3.79	14.29	13.78	20.5		Reiners et al. (2012)
J12141654+0037263	GJ 1154	6.110	4.19	6.63	5.14	6.0		Reiners et al. (2009)
J12185939+1107338	GJ 1156	6.328	4.36	11.58	10.73	15.5	1.6	Reiners et al. (2017)
J13003350+0541081	Gl 493.1	5.774	3.99	11.85	11.16	16.4	1.6	Reiners et al. (2017)
J13004666+1222325	Gl 494	4.131	4.00	8.34	7.32	9.7		Browning et al. (2010)
J13295979+1022376	Gl 514	4.049	4.05	4.06	0.32	1.5		Reiners (2007)
J13314666+2916368	GJ 3789*	5.273	3.81	47.89	47.74	55.5	8.4	Reiners et al. (2017)
J13454354+1453317	Gl 526	4.075	4.03	4.01		2.0		Reiners (2007)
J14172209+4525461		5.465	3.86	13.69	13.13	15.9	1.6	Reiners et al. (2017)
J15215291+2058394	GJ 9520	4.337	3.91	6.12	4.71	4.3	1.5	Reiners et al. (2017)
J15303032+0926014	NLTT 40406	6.485	4.50	6.41	4.57	16.3	1.6	Reiners et al. (2017)
J15553178+3512028	G 180-11	5.617	3.92			21.9		Jenkins et al. (2009)
J16301808−1239434	Gl 628	5.043	3.79	3.87	0.77	1.5		Reiners (2007)
J16352740+3500577	GJ 3966	5.163	3.80			15.8		Reiners et al. (2012)
J16553529−0823401	Gl 644C	6.798	4.82	10.26	9.05	5.4	1.5	Reiners et al. (2017)
J16570570−0420559	GJ 1207	5.159	3.80	9.23	8.41	10.7		Reiners et al. (2012)
J18021660+6415445	G 227-22	5.721	3.96	11.68	10.99	11.3	1.5	Reiners et al. (2017)
J18073292−1557464	GJ 1224	5.711	3.96	6.23	4.81	2.2	1.5	Reiners et al. (2017)
J18130657+2601519	GJ 4044	5.193	3.80	7.89	6.92	5.9	1.5	Reiners et al. (2017)
J18185725+6611332	GJ 4053	5.495	3.87	11.57	10.90	15.3	1.5	Reiners et al. (2017)
J19165762+0509021	Gl 752B	6.937	4.98	8.40	6.76	2.7	2.2	Reiners et al. (2017)
J19510930+4628598	GJ 1243	5.188	3.80	15.08	14.59	22.5	2.3	Reiners et al. (2017)
J19535508+4424550	GJ 1245B	6.603	4.61	8.15	6.72	7.0		Reiners & Basri (2007)
J20294834+0941202	Gl 791.2*	5.757	3.98	21.17	20.80	32.0	2.0	Delfosse et al. (1998)
J22011310+2818248	GJ 4247*	5.228	3.81	21.42	21.08	35.4	3.5	Reiners et al. (2017)
J22464980+4420030	Gl 873	4.963	3.79	7.00	5.88	3.5	1.5	Reiners et al. (2017)
J22515348+3145153	Gl 875.1	4.726	3.80	10.28	9.55	13.4	1.5	Reiners et al. (2017)
J23292258+4127522	GJ 4338B*	5.274	3.81	9.17	8.34	14.5		Reiners et al. (2012)
J23315208+1956142	Gl 896A	4.857	3.79	11.06	10.39	17.5		Morin et al. (2008b)
J23315244+1956138	Gl 896B*	5.938	4.08	16.47	15.96	24.2	1.4	Delfosse et al. (1998)
J23545147+3831363		5.097	3.79	6.94	5.81	3.6	1.5	Reiners et al. (2017)

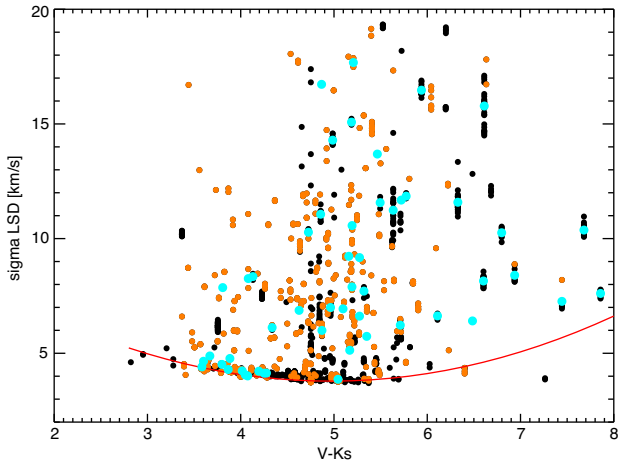

Figure 7. Variation of the LSD profile width with colour, with the adopted lower envelope fit (red line). Black points correspond to polarimetric measurements and orange points to S+S spectra. Calibrators are marked with large cyan filled circles.

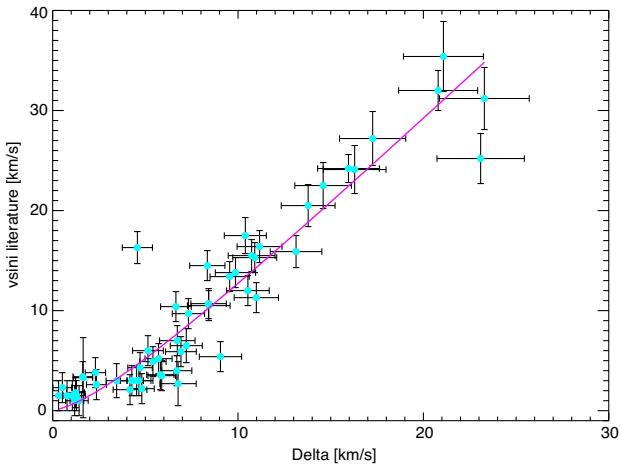

Figure 8. Literature value of $v \sin i$ with respect to the measured width attributed to rotation. A fit given by equation (3) is overplotted.

5.3 Second approach: measure of the 995.0334 nm FeH line

We have selected two FeH lines recommended by Reiners (2007), because the continuum is well defined around 1 μm and these two lines are insensitive to gravity and magnetic effects. However, Reiners (2007) used the Coudé Echelle Spectrograph (CES) at La Silla Observatory (Chile), which has a resolution of 200 000. ESPaDOnS in polarimetric mode has a typical resolution of 65 000 and one of the Reiners' line is blended in our spectra. We therefore only measure the FeH line at 995.0334 nm (air wavelength), which is very well defined in most of our spectra.

We fit a Gaussian with a linear baseline to this line, and estimate the quality of the fit using various criteria. In some cases, the fit produces spurious results, for instance for spectroscopic binaries, low S/N spectra, K dwarfs where the FeH lines tend to disappear, etc. The criteria are:

(i) the wavelength shift with respect to the expected position must be smaller than 0.02 nm;

(ii) the value of the χ^2 per degrees of freedom must be smaller than 0.7;

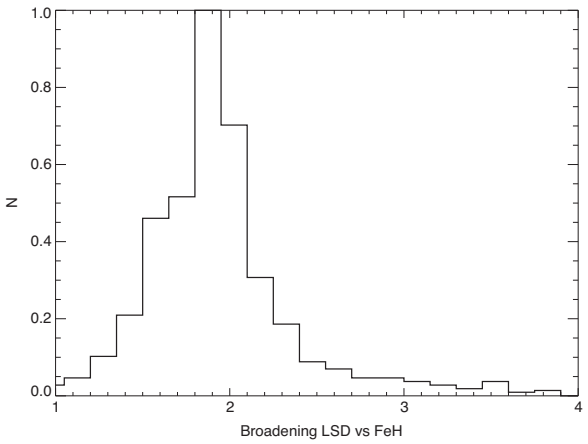

Figure 9. Histogram of the broadening of the LSD profile with respect to the 995.0334 nm FeH line, displayed as the ratio of the widths.

(iii) the signal must be in absorption and its amplitude must be large enough compared to the noise: after fitting the Gaussian profile, we subtract it from the spectrum and measure the residual noise: we accept a line if the ratio of its amplitude to the noise is larger than 3;

(iv) finally, we reject the fit when the σ is smaller than 1 pixel or much larger than the corresponding σ of the LSD profile by a factor 3.

With these criteria, about 865 of our 1900 spectra provide a valuable fit of the 995.0334 nm FeH line.

A comparison of the LSD profile widths σ to the corresponding values for the FeH line is shown as a histogram of the corresponding broadening in Fig. 9, displayed as the ratio of the widths. It appears that in average the LSD profile is about twice larger than a single FeH line. We checked that this ratio does not significantly depend of the colour of the star.

This result is confirmed by an analysis of a BT-Settl synthetic spectrum at $T_{\rm eff} = 3500$ K, [Fe/H]=0.0, and $\log g = 5.0$, where we measure an average line width of 0.24 nm for 3 Ti I lines around 974 nm, and 0.11 nm for 2 FeH lines around 993 nm. A possible interpretation of this difference in line widths between atomic lines and molecular FeH lines comes from the low dissociation energy of FeH, namely 1.63 eV. So the molecule will be dissociated in regions where the turbulence is strong. A quick calculation gives a corresponding collision velocity of 2.4 km s^{-1}. Higher velocity collisions would destroy the molecule and reduce the pressure broadening accordingly.

A similar diagram to Fig. 7 for the FeH line is displayed in Fig. 10 and shows a lower envelope which is flatter than for the LSD profile width and not defined very accurately, as a single line measurement is noisier than the LSD profile. This envelope is fit by equation (4):

$$3\sigma_\circ = 1.72 - 0.215\,(V-Ks) + 0.0352\,(V-Ks)^2 \pm 0.48 \pm 0.187 \pm 0.0168. \quad (4)$$

The corresponding calibration of $v \sin i$ versus Δ as defined in equation (2) can be fit by a similar formula to equation (3), but we find in practice that a linear fit is accurate enough. It is given by equation (5) and shown in Fig. 11:

$$2v \sin i = -3.14 + 2.48\,\Delta \pm 0.59 \pm 0.13. \quad (5)$$

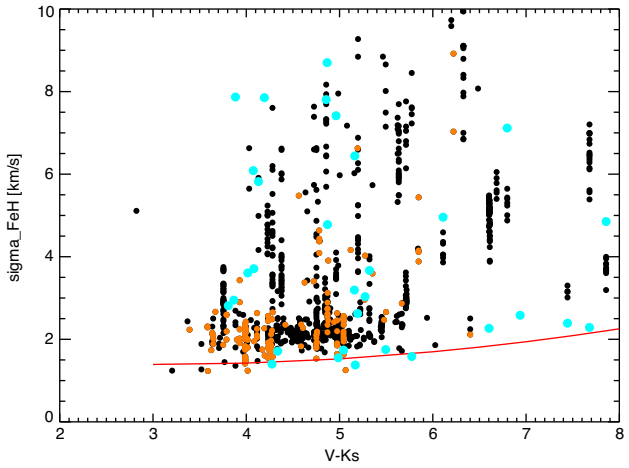

Figure 10. Variation of the 995.0334 nm FeH line width with colour, with the adopted lower envelope fit (red line). Symbols are the same as in Fig. 7.

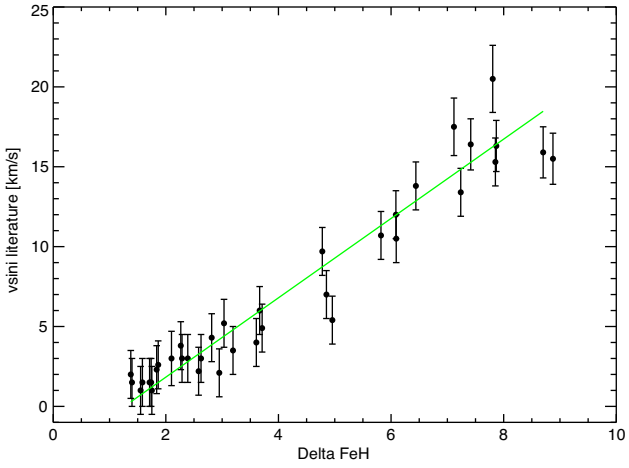

Figure 11. Literature value of $v\sin i$ with respect to the measured width of the 995.0394 nm FeH line, attributed to rotation. A linear fit is used for the calibration.

Table 7. List of slow rotators used as templates in the alternative technique, with their adopted values of $v\sin i$ in $\mathrm{km\,s^{-1}}$, and the S/N of the spectrum.

Common name	Spectral type	$v\sin i$	S/N
Gl 273	M3.5	1.0	499
Gl 382	M1.5	1.8	297
Gl 393	M2.0	1.5	356
Gl 514	M1.0	1.5	293
Gl 526	M1.5	2.0	433
Gl 628	M3.5	1.5	219

5.4 Third approach: convolution with slow rotator templates

A different technique consists in using a few slow rotators with high S/N spectra obtained with ESPaDOnS and for which the value of $v\sin i$ is well measured by high S/N spectra at higher resolution. The method is described in details in Malo et al. (2014b) and uses six calibrators, ranging in spectral type from M1.0 to M3.5, listed in Table 7. The reference values of $v\sin i$ all come from Reiners (2007), who used very high-resolution spectra (200 000) from the CES spectrograph at La Silla Observatory, which ensures reliability and homogeneity. The S/N of the ESPaDOnS spectrum used as template is given in the last column of Table 7, and is measured per CCD pixel at 810 nm on the intensity spectrum.

For each calibrator, we artificially broaden its spectrum using different values of $v\sin i$, and for each star in our sample, we look for the best fit of its spectrum among the library of broadened spectra of the calibrators. We then adopt as the value of $v\sin i$ for this spectrum the best match.

A comparison of the results of this technique with the value of $v\sin i$ calibrated from the measure of the width of the LSD profile gives a good agreement at intermediate projected rotation velocity (typically from 4 to 30 $\mathrm{km\,s^{-1}}$). For slower rotators, there are differences due both to the calibration of $\sigma_\circ$ for the LSD profile method, and the adopted template RV for the template method. For rapid rotators (and a few specific stars such as Gl 412B), non-Gaussian LSD profiles affect both methods and lead to differences between the two approaches too.

5.5 Adopted projected rotation velocity

From the three methods exposed above, we adopt a value of $v\sin i$ which is defined as follows, where $v\sin i_{\mathrm{LSD}}$ is obtained from the calibrated LSD intensity profile, $v\sin i_{\mathrm{FeH}}$ from the FeH line, and $v\sin i_{\mathrm{c}}$ from the template convolution:

(i) All three methods are used and compared for each star, with the goal of obtaining a single value per star with an error bar representative of data quality, measurement dispersion, and calibration uncertainties.

(ii) The median value of the three measurement is adopted, when $v\sin i_{\mathrm{LSD}}$ is larger than 3 $\mathrm{km\,s^{-1}}$ (resolved profiles) and $v\sin i_{\mathrm{FeH}}$ is measured.

(iii) When $v\sin i_{\mathrm{LSD}}$ is smaller than 3 $\mathrm{km\,s^{-1}}$ (unresolved profiles), $v\sin i_{\mathrm{c}}$ is not included in the adopted value calculation.

(iv) When $v\sin i_{\mathrm{LSD}}$ was found smaller than 2 $\mathrm{km\,s^{-1}}$, we estimate that the rotation profile is unresolved in ESPaDOnS spectra and such values are reported as '<2'.

For stars with a strong magnetic field, $v\sin i_{\mathrm{FeH}}$ from the FeH line should be preferred over the other two methods, as it is insensitive to the magnetic field. However, as the measurement is based on a single line it is more noisy, and in addition these stars are generally rapid rotators, which makes the line blended with nearby lines.

6 DISCUSSION

6.1 Comparison between projected and equatorial rotation velocities

We found about 150 stars in our sample with a known rotation period, either measured from time series photometry or spectroscopy of chromospheric indicators (Suárez Mascareño et al. 2015). We did not use rotation periods deduced from spectroscopic measurements when they are converted from chromospheric indicators such as R'_{HK} or projected rotation velocities $v\sin i$. Uncertain values are given in parentheses. From this period and the adopted radius of the star, we compute the equatorial rotation velocity, using $v_{\mathrm{eq}} = 50.59\,R/P_{\mathrm{rot}}$, where v_{eq} is in $\mathrm{km\,s^{-1}}$, R in $\mathcal{R}_\odot^{\mathrm{N}}$ (assumed to be 695 700 km from Prša et al. 2016), and P_{rot} in days. An alternative approach pioneered e.g. by Donati et al. (2008) consists in comparing $R\sin i$ to the adopted radius, under the hypothesis that $v\sin i$ is measured more accurately than R, at least for rapid rotators. In our case, $v\sin i$ depends on the adopted calibrations and averaging process, so it

is probably not more accurate than the star radius, which is estimated from the star colour $V - J$ by a relation that we calibrated on interferometrically measured radii from Boyajian et al. (2012).

We divided our sample into two parts; the slow rotators ($v_{\rm eq} < 3\,{\rm km\,s^{-1}}$), for which we want to check that small equatorial velocities are confirmed by a small value of $v\sin i$ from our measurement, and the resolved rotators, for which our measurement of $v\sin i$ should be smaller than the computed $v_{\rm eq}$. Both tables are given in Appendix A.

We confirm that the calculus of $v_{\rm eq}$ from the estimated radius and measured $P_{\rm rot}$ agrees with our measured value of $v\sin i$ for average inclinations: about two-thirds of the expected slow rotators are not resolved with our spectrograph ($v\sin i < 2\,{\rm km\,s^{-1}}$). Those having a measured value of $v\sin i$ may indicate that our calibration is slightly inaccurate (supposedly resolved projected rotation velocities are in fact upper limits). In a few cases, it may be due to a metallicity effect in the calibration of equations (1) and (4), which has not been taken into account and may affect metal-poor and metal-rich stars (see Melo et al. 2001, for an explanation of this expected effect).

However, in about half the cases of resolved rotators, $v\sin i$ taken at face value is larger than $v_{\rm eq}$. It is not unexpected that the distribution of $\sin i$ is biased towards larger values, as there is an observational bias against low inclination systems where photometric variations are more difficult to detect. However, the magnitude of the effect is too large to be attributed to this bias. This surprising effect has already been evidenced by e.g. Reiners et al. (2012, see their fig. 10), who attribute it to possibly inaccurate photometric rotation periods. We can also add inaccurate radii, for instance for young stars, as we use a mean relation only valid for old stars. But these inaccuracies can probably only explain a few cases, not the majority.

6.2 From fundamental properties to radial-velocity uncertainty

Using the measured effective temperatures and collected apparent magnitudes in the H band, it was then possible to estimate the potential of SPIRou observations for this sample of stars. When effective temperatures were not available, we used first the values from Mann et al. (2015), then their equation (7) deriving $T_{\rm eff}$ from the $V - J$ colour index and a correction for unknown metallicity based on the $J - H$ colour index, with coefficients given in their table 2. We then use an exposure simulator for SPIRou to estimate the S/N obtained in a typical visit of 600 s integration time, with median seeing conditions of Maunakea (0.6 arcsec in the H band). Then, from the S/N estimates, we used the RV content as calculated in Figueira et al. (2016) to estimate the range of RV uncertainties per visit. The quantity depends upon the rotational velocity, the effective temperature, and the performance of telluric corrections, in addition to the S/N. In Fig. 12, we show two extreme conditions for each star where an effective temperature and rotational velocity are available: the conservative configuration where all regions contaminated by telluric lines more than 2 per cent depth are masked, and the optimistic configuration where these telluric lines are almost completely corrected for (see details in Figueira et al. 2016, their cases 2 and 3). It is difficult, at this point, to predict where telluric corrections with SPIRou will stand: the proposed method is a Principal Component Analysis (PCA)-based approach using a library of observed telluric spectra in varying conditions (Artigau et al., 2014); its performance in real conditions still needs to be assessed. As a first estimate, we used the RV uncertainty calculated for a rotational velocity of 1 (respectively, 10) km s^{-1} for all stars having a $v\sin i$ less than (respectively, greater than) 5 km s^{-1}, which explains why data points are not covering the parameter space randomly.

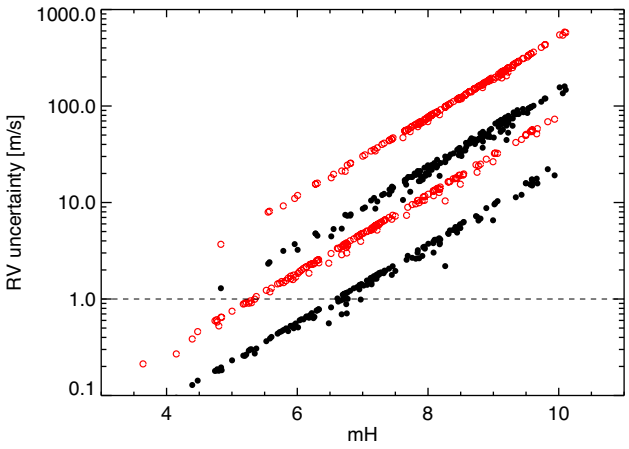

Figure 12. The expected RV uncertainty that would be achieved with SPIRou in 600 s exposures, as a function of the stellar magnitude. A range of values for a given magnitude is obtained, depending on the performance of telluric corrections (from black: optimistic to red: conservative). The two different black and red sequences roughly mimic rapid (10 km s^{-1}, upper sequence) and slow (1 km s^{-1}, lower sequence) rotator cases. The horizontal line shows a realistic noise floor for such observations.

Finally, as the RV uncertainty is derived by photometric band, we applied the correction factor found for Barnard's star between models and observations of this M4 star (Artigau et al. submitted). These correction factors enhance the contribution of the H and K bands with respect to the bluer part of the spectrum; it is not yet known how they vary across the spectral type of M stars and with their metallicity.

Fig. 12 shows that an RV uncertainty of 1 m s^{-1} is achieved for all slowly rotating stars brighter than an H magnitude of 7 in 600 s. Fainter stars, or faster rotators, would need a longer exposure time to achieve this precision. When the conservative approach of telluric masking is used, the limit drops by almost two magnitudes, showing the importance of devoting telescope time and pipeline development efforts to recover the stellar signal in these contaminated area. Finally, it seems that stars rotating at more than 10 km s^{-1} will never achieve the 1 m s^{-1} level, even when perfect telluric corrections are applied, down to an H magnitude of 4.5. This must be taken into account when considering the targets for planet searches.

6.3 Multiplicity and planet formation

Among the 153 systems listed in Table A2, more than half (88) have an apparent separation smaller than 2.0 arcsec, preventing in most cases a clear separation of the two components with our instruments, the fibre of which have diameters of 1.6 arcsec (ESPaDOnS) and 1.2 arcsec (SPIRou). Thebault & Haghighipour (2014) warn that RV surveys aiming at exoplanet detection reject binary systems and therefore prevent from getting information about the planet formation in such systems. They mention a physical separation of about 100 au below which the planet formation is affected. For the above-mentioned limit in angular separation (2.0 arcsec), this corresponds to a distance from Earth to the multiple system of 50 pc.

A more complete statistics has been drawn from our catalogue of multiple systems involving an M dwarf. Among 669 systems, 111

have a physical separation smaller than 100 au (assuming they are all physical systems). Among those, 28 are close enough to have an angular separation larger than 2.0 arcsec. This means that our observational constraints typically reject 75 per cent of the interesting sample where planet formation may be affected by the binarity.

Spectroscopic binaries are also rejected from most samples, especially SB2. In our sample of 440 M dwarfs, we listed 55 SB2 already known or discovered by us, a rate of 12.5 per cent. About a third of them are also close visual binaries (angular separation smaller than 2.0 arcsec), allowing a good determination of their physical properties.

In summary, about 80 per cent of interesting multiple systems for constraining the planet formation mechanism are lost to the size of the spectrograph fibers, linked to the atmospheric seeing.

7 SUMMARY AND CONCLUSION

In this paper, we have been reporting on a sample of 440 M dwarfs observed with the ESPaDOnS spectropolarimeter at CFHT. 114 of them correspond to observations conducted by our team in the framework of the CoolSnap collaboration. Two other papers (Moutou et al. 2017; Malo et al., in preparation) report additional results from this program. Another 71 stars observed in polarimetric mode and 255 in spectroscopic mode (S+S) were extracted from the ESPaDOnS archive at CADC and cover the whole set of observations of M dwarfs conducted at CFHT between 2005 and 2015.

From this homogeneous set of observations, we measured spectral type using the TiO_5 index, effective temperatures and metallicities using the MCAL method when the star is not active (Hα index smaller than 0.25, see Section 4). We checked that our values generally agree with measurements obtained from similar or different methods in the literature.

As part of a larger project to identify multiple systems involving M dwarfs, we list all the stars in our sample belonging to such system, without limit on the separation. We also identify new spectroscopic binaries from our observations and summarize those already known from the literature.

We calibrate the measurement of the projected rotation velocity from the width of the LSD profile. This calibration is valid for other observations of late-type dwarfs observed with the ESPaDOnS spectropolarimeter.

Finally, we estimate the RV content for each star of our sample, in order to select those which are expected to display the smallest RV uncertainty possible with SPIRou. This work participates to the effort of selecting the targets for low-mass planet search using the new high-velocity precision near-infrared spectropolarimeter SPIRou. In the first paper, Moutou et al. (2017) defined a merit function based on the star activity; in this paper, we discarded close binaries and estimated the expected RV uncertainty; in the final paper of this series, Malo et al. (in preparation) use the present measurements of $T_{\rm eff}$ and [Fe/H] to refine the planet-detection merit function used to define the initial sample, and combines it to the other merit function and selection criteria to finally select the best sample of targets for the new SPIRou instrument.

ACKNOWLEDGEMENTS

The authors wish to recognize and acknowledge the very significant cultural role that the summit of Maunakea has always had within the indigenous Hawaiian community. We are most grateful to have the opportunity to conduct observations from this mountain.

We are sincerely grateful to the anonymous referee, whose careful reading and suggested additions and corrections helped and clarified the paper.

PF gratefully acknowledges Simon Prunet's help with the PYTHON codes and the entire CFHT 'Ohana' for offering excellent conditions of work.

This research has made use of:

(i) the Set of Identifications, Measurements and Bibliography for Astronomical Data (SIMBAD) data base and the VizieR catalogue access tool, operated at CDS, Strasbourg, France. The original description of the SIMBAD data base was published in A&AS, 143, 9 (2000), and of the VizieR service in A&AS, 143, 23 (2000);

(ii) data products from the 2MASS, which is a joint project of the University of Massachusetts and the Infrared Processing and Analysis Center/California Institute of Technology, funded by the National Aeronautics and Space Administration and the National Science Foundation;

(iii) data products from the AAVSO Photometric All Sky Survey, funded by the Robert Martin Ayers Sciences Fund and the National Science Foundation;

(iv) data from the European Space Agency mission *Gaia* (http://www.cosmos.esa.int/gaia), processed by the *Gaia* Data Processing and Analysis Consortium (DPAC) (http://www.cosmos.esa.int/web/gaia/dpac/consortium). Funding for the DPAC has been provided by national institutions, in particular the institutions participating in the *Gaia* Multilateral Agreement;

(v) the facilities of the CADC operated by the National Research Council of Canada with the support of the Canadian Space Agency;

(vi) the Washington Double Star Catalog maintained at the U.S. Naval Observatory.

This research has made use of the Brazilian time at CFHT through the agreement between the Brazilian Ministry of Science Technology Innovation and Communications (MCTIC) and the CFHT. EM acknowledges the support of CNPq, under the Universal grant process number 443557/2014-4, and also the support of FAPEMIG, under project number 01/2014-23092.

XD, TF, and FA received funding from the French Programme National de Physique Stellaire and the Programme National de Planétologie of CNRS (INSU). This work has been partially supported by the Labex OSUG@2020. The computations of atmosphere models were performed in part on the Milky Way supercomputer, which is funded by the Deutsche Forschungsgemeinschaft through the Collaborative Research Centre (SFB 881) 'The Milky Way System' (sub-project Z2) and hosted at the University of Heidelberg Computing Centre, and at the Pôle Scientifique de Modélisation Numérique at the École Normale Supérieure in Lyon, and at the Gesellschaft für Wissenschaftliche Datenverarbeitung Göttingen in collaboration with the Institut für Astrophysik Göttingen. This is also based on observations obtained at the CFHT which is operated by the National Research Council of Canada, the Institut National des Sciences de l'Univers of the Centre National de la Recherche Scientifique of France, and the University of Hawaii.

REFERENCES

Allard F., Homeier D., Freytag B., Schaffenberger W., Rajpurohit A. S., 2013, Mem. Soc. Astron. Ital. Suppl., 24, 128
Alonso-Floriano F. J. et al., 2015, A&A, 577, A128
Artigau É. et al., 2014, Proc. SPIE, 9149, p. 914905
Baize P., 1976, A&AS, 26, 177

Barnes J. R., Jeffers S. V., Haswell C. A., Jones H. R. A., Shulyak D., Pavlenko Y. V., Jenkins J. S., 2017, MNRAS, 471, 811
Becklin E. E., Zuckerman B., 1988, Nature, 336, 656
Benedict G. F., McArthur B. E., Franz O. G., Wasserman L. H., Henry T. J., 2000, AJ, 120, 1106
Bergfors C. et al., 2010, A&A, 520, A54
Beuzit J.-L. et al., 2004, A&A, 425, 997
Bieger Smith G. S., 1964, AJ, 69, 804
Blackwell D. E., Petford A. D., Arribas S., Haddock D. J., Selby M. J., 1990, A&A, 232, 396
Boisse I. et al., 2010, A&A, 523, A88
Bonfils X., Delfosse X., Udry S., Santos N. C., Forveille T., Ségransan D., 2005, A&A, 442, 635
Bonfils X. et al., 2013, A&A, 549, A109
Bowler B. P., Liu M. C., Shkolnik E. L., Dupuy T. J., Cieza L. A., Kraus A. L., Tamura M., 2012, ApJ, 753, 142
Bowler B. P., Liu M. C., Shkolnik E. L., Tamura M., 2015a, ApJS, 216, 7
Bowler B. P. et al., 2015b, ApJ, 806, 62
Boyajian T. S. et al., 2012, ApJ, 757, 112
Brandt T. D. et al., 2014, ApJ, 786, 1
Browning M. K., Basri G., Marcy G. W., West A. A., Zhang J., 2010, AJ, 139, 504
Casagrande L., Flynn C., Bessell M., 2008, MNRAS, 389, 585
Claudi R. et al., 2016, Proc. SPIE, 9908, 99081A
Cortés-Contreras M. et al., 2017, A&A, 597, A47
Daemgen S., Siegler N., Reid I. N., Close L. M., 2007, ApJ, 654, 558
Davison C. L. et al., 2014, AJ, 147, 26
Deeg H., Belmonte J., 2018, Handbook of Exoplanets. Handbook of Exoplanets, Springer International Publishing, Berlin, https://books.google.com/books?id=Gq1LnQAACAAJ
Delfosse X., Forveille T., Perrier C., Mayor M., 1998, A&A, 331, 581
Delfosse X., Forveille T., Mayor M., Burnet M., Perrier C., 1999a, A&A, 341, L63
Delfosse X., Forveille T., Beuzit J.-L., Udry S., Mayor M., Perrier C., 1999b, A&A, 344, 897
Delfosse X. et al., 2013, A&A, 553, A8
Dommanget J., Nys O., 2000a, A&A, 363, 991
Dommanget J., Nys O., 2000b, A&A, 364, 927
Donati J.-F., Semel M., Carter B. D., Rees D. E., Collier Cameron A., 1997, MNRAS, 291, 658
Donati J.-F., Forveille T., Collier Cameron A., Barnes J. R., Delfosse X., Jardine M. M., Valenti J. A., 2006, Science, 311, 633
Donati J.-F. et al., 2008, MNRAS, 390, 545
Engle S. G., Guinan E. F., Mizusawa T., 2009, in van Steenberg M. E., Sonneborn G., Moos H. W., Blair W. P., eds, AIP Conf. Ser. Vol. 1135, Future Directions in Ultraviolet Spectroscopy. Am. Inst. Phys., New York, p. 221
Epchtein N. et al., 1999, A&A, 349, 236
Figueira P. et al., 2016, A&A, 586, A101
Frith J. et al., 2013, MNRAS, 435, 2161
Gaidos E. et al., 2014, MNRAS, 443, 2561
Gizis J. E., Reid N. I., 1996, AJ, 111, 365
Goldin A., Makarov V. V., 2007, ApJS, 173, 137
Goldman B., Marsat S., Henning T., Clemens C., Greiner J., 2010, MNRAS, 405, 1140
Gomes da Silva J., Santos N. C., Bonfils X., Delfosse X., Forveille T., Udry S., 2011, A&A, 534, A30
Gould A., Chanamé J., 2004, ApJS, 150, 455
Harrington R. S., Dahn C. C., 1984, IAU Circ., 3989, 1
Hartkopf W. I., McAlister H. A., Mason B. D., Barry D. J., Turner N. H., Fu H.-H., 1994, AJ, 108, 2299
Hartman J. D., Bakos G. Á., Noyes R. W., Sipőcz B., Kovács G., Mazeh T., Shporer A., Pál A., 2011, AJ, 141, 166
Hauschildt P. H., Allard F., Ferguson J., Baron E., Alexander D. R., 1999, ApJ, 525, 871
Heintz W. D., 1994, AJ, 108, 2338
Herbig G. H., Moorhead J. M., 1965, ApJ, 141, 649
Houdebine E. R., Mullan D. J., 2015, ApJ, 801, 106
Huélamo N. et al., 2008, A&A, 489, L9
Irwin J., Berta Z. K., Burke C. J., Charbonneau D., Nutzman P., West A. A., Falco E. E., 2011, ApJ, 727, 56
Janson M. et al., 2012, ApJ, 754, 44
Janson M., Bergfors C., Brandner W., Kudryavtseva N., Hormuth F., Hippler S., Henning T., 2014, ApJ, 789, 102
Jenkins J. S., Ramsey L. W., Jones H. R. A., Pavlenko Y., Gallardo J., Barnes J. R., Pinfield D. J., 2009, ApJ, 704, 975
Jódar E., Pérez-Garrido A., Díaz-Sánchez A., Villó I., Rebolo R., Pérez-Prieto J. A., 2013, MNRAS, 429, 859
Johnson J. A., Apps K., 2009, ApJ, 699, 933
Joy A. H., Sanford R. F., 1926, ApJ, 64
Karataş Y., Bilir S., Eker Z., Demircan O., 2004, MNRAS, 349, 1069
Kiraga M., 2012, Acta Astron., 62, 67
Kiraga M., Stepien K., 2007, Acta Astron., 57, 149
Kiraga M., Stępień K., 2013, Acta Astron., 63, 53
Kirkpatrick J. D., 2000, in Griffith C. A., Marley M. S., eds, ASP Conf, Ser. Vol. 212, From Giant Planets to Cool Stars. Astron. Soc. Pac., San Francisco, p. 20
Kirkpatrick J. D. et al., 1999, ApJ, 519, 802
Kirkpatrick J. D. et al., 2012, ApJ, 753, 156
Kurucz R., 1993a, ATLAS9 Stellar Atmosphere Programs and 2 km/s grid. Kurucz CD-ROM No. 13. Smithsonian Astrophysical Observatory, Cambridge, MA, p. 13
Kurucz R., 1993b, SYNTHE Spectrum Synthesis Programs and Line Data. Kurucz CD-ROM No. 18. Smithsonian Astrophysical Observatory, Cambridge, MA, p. 18
Law N. M., Hodgkin S. T., Mackay C. D., 2006, MNRAS, 368, 1917
Law N. M., Hodgkin S. T., Mackay C. D., 2008, MNRAS, 384, 150
Lépine S., Bongiorno B., 2007, AJ, 133, 889
Lépine S., Gaidos E., 2011, AJ, 142, 138
Lépine S., Rich R. M., Shara M. M., 2007, ApJ, 669, 1235
Leung K.-C., Schneider D. P., 1978, AJ, 83, 618
Lindgren S., Heiter U., 2017, A&A, 604, A97
Lindgren S., Heiter U., Seifahrt A., 2016, A&A, 586, A100
Lippincott S. L., 1977, AJ, 82, 925
Mahadevan S. et al., 2012, Proc. SPIE, 8446, 84461S
Makarov V. V., Kaplan G. H., 2005, AJ, 129, 2420
Maldonado J. et al., 2015, A&A, 577, A132
Malo L., Artigau É., Doyon R., Lafrenière D., Albert L., Gagné J., 2014a, ApJ, 788, 81
Malo L., Doyon R., Feiden G. A., Albert L., Lafrenière D., Artigau É., Gagné J., Riedel A., 2014b, ApJ, 792, 37
Mann A. W., Brewer J. M., Gaidos E., Lépine S., Hilton E. J., 2013a, AJ, 145, 52
Mann A. W., Gaidos E., Ansdell M., 2013b, ApJ, 779, 188
Mann A. W., Feiden G. A., Gaidos E., Boyajian T., von Braun K., 2015, ApJ, 804, 64
Martin E. L., Basri G., Delfosse X., Forveille T., 1997, A&A, 327, L29
Martín E. L., Delfosse X., Basri G., Goldman B., Forveille T., Zapatero Osorio M. R., 1999, AJ, 118, 2466
Martinache F., Lloyd J. P., Ireland M. J., Yamada R. S., Tuthill P. G., 2007, ApJ, 661, 496
Mason B. D., Wycoff G. L., Hartkopf W. I., Douglass G. G., Worley C. E., 2001, AJ, 122, 3466
McCarthy C., Zuckerman B., Becklin E. E., 2001, AJ, 121, 3259
Melo C. H. F., Pasquini L., De Medeiros J. R., 2001, A&A, 375, 851
Montagnier G. et al., 2006, A&A, 460, L19
Morin J. et al., 2008a, MNRAS, 384, 77
Morin J. et al., 2008b, MNRAS, 390, 567
Morin J., Donati J.-F., Petit P., Delfosse X., Forveille T., Jardine M. M., 2010, MNRAS, 407, 2269
Morin J. et al., 2011, in Prasad Choudhary D., Strassmeier K. G., eds, IAU Symp. Vol. 273, Physics of Sun and Star Spots. Kluwer, Dordrecht, p. 181
Moutou C. et al., 2007, A&A, 473, 651
Moutou C. et al., 2017, MNRAS, 472, 4563
Nakajima T., Oppenheimer B. R., Kulkarni S. R., Golimowski D. A., Matthews K., Durrance S. T., 1995, Nature, 378, 463

Nelson B. E., Robertson P. M., Payne M. J., Pritchard S. M., Deck K. M., Ford E. B., Wright J. T., Isaacson H. T., 2016, MNRAS, 455, 2484
Neves V. et al., 2012, A&A, 538, A25
Neves V., Bonfils X., Santos N. C., Delfosse X., Forveille T., Allard F., Udry S., 2013, A&A, 551, A36
Neves V., Bonfils X., Santos N. C., Delfosse X., Forveille T., Allard F., Udry S., 2014, A&A, 568, A121
Newton E. R., Charbonneau D., Irwin J., Berta-Thompson Z. K., Rojas-Ayala B., Covey K., Lloyd J. P., 2014, AJ, 147, 20
Newton E. R., Irwin J., Charbonneau D., Berta-Thompson Z. K., Dittmann J. A., West A. A., 2016, ApJ, 821, 93
Newton E. R., Irwin J., Charbonneau D., Berlind P., Calkins M. L., Mink J., 2017, ApJ, 834, 85
Nidever D. L., Marcy G. W., Butler R. P., Fischer D. A., Vogt S. S., 2002, ApJS, 141, 503
Norton A. J. et al., 2007, A&A, 467, 785
Önehag A., Heiter U., Gustafsson B., Piskunov N., Plez B., Reiners A., 2012, A&A, 542, A33
Pettersen B. R., Coleman L. A., Evans D. S., 1984, ApJ, 282, 214
Prša A. et al., 2016, AJ, 152, 41
Quirrenbach A. et al., 2014, Proc. SPIE, 9147, 91471F
Rajpurohit A. S., Reylé C., Allard F., Homeier D., Schultheis M., Bessell M. S., Robin A. C., 2013, A&A, 556, A15
Rajpurohit A. S., Allard F., Teixeira G. D. C., Homeier D., Rajpurohit S., Mousis O., 2017, A&A, preprint (arXiv:1708.06211)
Rebolo R., Zapatero Osorio M. R., Martín E. L., 1995, Nature, 377, 129
Reid I. N., Gizis J. E., 1997, AJ, 113, 2246
Reid I. N., Hawley S. L., Gizis J. E., 1995, AJ, 110, 1838
Reiners A., 2007, A&A, 467, 259
Reiners A., Basri G., 2007, ApJ, 656, 1121
Reiners A., Basri G., Browning M., 2009, ApJ, 692, 538
Reiners A., Joshi N., Goldman B., 2012, AJ, 143, 93
Reiners A. et al., 2017, A&A, preprint (arXiv:1711.06576)
Reuyl D., 1943, ApJ, 97, 186
Robertson P., Mahadevan S., Endl M., Roy A., 2014, Science, 345, 440
Rojas-Ayala B., Covey K. R., Muirhead P. S., Lloyd J. P., 2012, ApJ, 748, 93
Schlaufman K. C., Laughlin G., 2010, A&A, 519, A105
Shkolnik E., Liu M. C., Reid I. N., Hebb L., Cameron A. C., Torres C. A., Wilson D. M., 2008, ApJ, 682, 1248
Shkolnik E., Liu M. C., Reid I. N., 2009, ApJ, 699, 649
Shkolnik E. L., Hebb L., Liu M. C., Reid I. N., Collier Cameron A., 2010, ApJ, 716, 1522
Shkolnik E. L., Anglada-Escudé G., Liu M. C., Bowler B. P., Weinberger A. J., Boss A. P., Reid I. N., Tamura M., 2012, ApJ, 758, 56
Skelly M. B., Unruh Y. C., Collier Cameron A., Barnes J. R., Donati J.-F., Lawson W. A., Carter B. D., 2008, MNRAS, 385, 708
Skrutskie M. F. et al., 2006, AJ, 131, 1163
Strand K. A., 1977, AJ, 82, 745
Suárez Mascareño A., Rebolo R., González Hernández J. I., Esposito M., 2015, MNRAS, 452, 2745
Suárez Mascareño A., Rebolo R., González Hernández J. I., 2016, A&A, 595, A12
Suárez Mascareño A. et al., 2017, A&A, 605, A92
Tamazian V. S., Docobo J. A., Balega Y. Y., 2008, in Hubrig S., Petr-Gotzens M., Tokovinin A., eds, ESO Astrophysics Symposia, Multiple Stars Across the H-R Diagram. Springer-Verlag, Berlin, Heidelberg, p. 71
Terrien R. C., Mahadevan S., Bender C. F., Deshpande R., Ramsey L. W., Bochanski J. J., 2012, ApJ, 747, L38
Terrien R. C., Mahadevan S., Deshpande R., Bender C. F., 2015, ApJS, 220, 16
Thebault P., Haghighipour N., 2014, in Jin S., Haghighipour N., Ip W.-H., eds, Planetary Exploration and Science: Recent Results and Advances, Springer, Berlin, p. 309
Tokovinin A. A., 1997, A&AS, 124
Tomkin J., Pettersen B. R., 1986, AJ, 92, 1424
Torres G., Stefanik R. P., Latham D. W., Mazeh T., 1995, ApJ, 452, 870
Torres C. A. O., Quast G. R., da Silva L., de La Reza R., Melo C. H. F., Sterzik M., 2006, A&A, 460, 695
van Gent H., 1926, Bull. Astron. Inst. Netherlands, 3, 121
Vinter Hansen J. M., 1940, PASP, 52, 329
Ward-Duong K. et al., 2015, MNRAS, 449, 2618
Watson C. L., 2006, in Society for Astronomical Sciences 25th Annual Symposium. Society for Astronomical Sciences, p. 47
West A. A. et al., 2004, AJ, 128, 426
West A. A., Weisenburger K. L., Irwin J., Berta-Thompson Z. K., Charbonneau D., Dittmann J., Pineda J. S., 2015, ApJ, 812, 3
Winters J. G. et al., 2015, AJ, 149, 5
Woolf V. M., Wallerstein G., 2005, MNRAS, 356, 963
Woolf V. M., Wallerstein G., 2006, PASP, 118, 218

SUPPORTING INFORMATION

Supplementary data are available at *MNRAS* online.

Table A6. Master list of data for the whole sample (440 dwarfs and 447 entries): number N of measured spectra, number n of rejected ones if any, instrument mode (P for polarimetry and/or S for S+S), spectral type (from TiO_5 index), $V - K_s$ colour, H magnitude, HRV, projected rotational velocity and error in $km\,s^{-1}$ (<2 if not resolved), Hα index, [Fe/H] and error, effective temperature and error in K, source code, RV uncertainty, and binarity flag (SB1, SB2, close VB).

Please note: Oxford University Press is not responsible for the content or functionality of any supporting materials supplied by the authors. Any queries (other than missing material) should be directed to the corresponding author for the article.

APPENDIX A:

Long tables of the paper are given in theses appendices.

A1 Table of double-line spectroscopic binaries

In Table A1 are listed all the SB2 systems in our sample, detected in this work and from the literature.

Table A1. Spectroscopic binaries detected in the observations of the CoolSnap sample, or listed in the literature and recovered from the ESPaDOnS archives (polarimetry and pure spectroscopy).

2MASS name	Common name	SB type	Reference
J00080642+4757025		SB2	Shkolnik et al. (2010)
J00424820+3532554	Gl 29.1A	SB2	This work
J01351393−0712517		SB2	Malo et al. (2014a)
J01434512−0602400		SB2	This work
J01451820+4632077	LHS 6032	SB2	Shkolnik et al. (2010)
J01591260+0331113	GJ 1041B	SB2	Shkolnik et al. (2010)
J02441245−1321387	LP 711-62	SB2	This work
J03371407+6910498	GJ 3236	SB2	Shkolnik et al. (2010)
J03373331+1751145	GJ 3239	SB2	Shkolnik et al. (2010)
J04134585−0509049	G 160-54	SB3	Bowler et al. (2015a)
J04244260−0647313		SB3	Shkolnik et al. (2010)
J05031607+2123563	HD 285190	SB2	This work
J06180730+7506032		SB3?	This work
J06573891+4951540		SB2	This work
J07100180+3831457	Gl 268	SB2	Tomkin & Pettersen (1986)
J07282116+3345127		SB2	Shkolnik et al. (2010); Malo et al. (2014a)
J07313848+4557173		SB2?	This work
J07343745+3152102	Gl 278C	DESB2	Leung & Schneider (1978)
J08313759+1923395	GJ 2069A	DESB2	Delfosse et al. (1999a)
J08585633+0828259	GJ 3522	SB2	Reid & Gizis (1997); Delfosse et al. (1999b)
J09091563−1236184		SB3	This work
J09201112−0110171	G 161-13	SB2	This work
J09361593+3731456		SB2	Malo et al. (2014a)
J10182870−3150029	TWA 6	SB2?	This work, but see Table 3
J10364812+5055041	G 196-37	SB2?	This work
J11220530−2446393	TWA 4	SB1+SB2	Karataş et al. (2004)
J11250052+4319393	LHS 2403	SB2?	This work, but see Table 3
J11515681+0731262		SB2	This work
J12165845+3109233	GJ 3719	SB2	this work
J12290290+4143497	GJ 3729	SB2(3?)	Shkolnik et al. (2012)
J12490273+6606366	Gl 487	SB3	Delfosse et al. (1999b)
J12521285+2908568	LP321-163	SB2?	This work
J14170294+3142472	GJ 3839	SB3	Delfosse et al. (1999b), Forveille (private communication)
J14493338−2606205	Gl 563.2A	SB2	This work
J15235385+5609320		SB2	This work
J16155939+3852102		SB2	This work
J16170537+5516094	Gl 616.2	SB2	Shkolnik et al. (2010)
J16411543+5344110		SB2?	This work
J16552880−0820103	Gl 644	SB2(3?)	Pettersen, Coleman & Evans (1984), Delfosse et al. (1999b)
J17035283+3211456	NLTT 44114	SB2?	This work
J17462934−0842362	G 20-13	SB2	Malo et al. (2014a)
J18410977+2447143	GJ 1230A	SB2	Gizis & Reid (1996); Delfosse et al. (1999b)
J18552740+0824090	Gl 735	SB2	Karataş et al. (2004)
J18561590+5431479	G 229-18	SB2	This work
J18580415−2953045	TYC 6872-1011-1	SB2?	This work
J19420065−2104051	LP 869-19	SB2	Malo et al. (2014a)
J20103444+0632140	NLTT 48838	SB2	Shkolnik et al. (2010)
J21000529+4004136	Gl 815	SB2	Karataş et al. (2004)
J21293671+1738353	Gl 829	SB2	Delfosse et al. (1999b)
J22143835−2141535	BD-22 5866	ESB2+SB2	Shkolnik et al. (2008)
J22384559−2037160	Gl 867A	SB2	Herbig & Moorhead (1965)
J23062378+1236269	G 67-46	SB2(3?)	Shkolnik et al. (2010)
J23172441+3812419	GJ 4327	SB2	Cortés-Contreras et al. (2017)
J23301341-2023271	GJ 1284	SB2	Torres et al. (2006)
J23435944+6444291	GJ 4359	SB2	Shkolnik et al. (2010)
J23483610-2739385	GJ 4362	SB2	Shkolnik et al. (2010)
J23584342+4643452	Gl 913	SB2?	This work

A2 Table of multiple systems involving M dwarfs in our sample

In Table A2, we list 153 multiple systems from this compilation and involving at least one of the M dwarfs of our sample, detected by imagery, with the level of multiplicity and the component we measured in parentheses following the WDS notation; we also give the most recent projected separation and the corresponding position angle, or the semimajor axis when the orbit is known; in that case, the position angle is listed as 'sma'; we list the physical status of the system (common proper motion and orbital monitoring), the year as given in the WDS, or the reference of discovery when more recent. For multiplicity larger than 2, we also list the separations and position angles for each pair composing the system (or the semimajor axes when 'sma' is listed as position angle), with a classical notation used to define the targeted pair (AB, Aab, Bab, etc.), following the WDS when possible. Twenty-three stars listed in Tables A1 and 2, which are only spectroscopic binaries are not repeated in this table, but spectroscopic binaries belonging to visual systems of higher multiplicity are included.

Table A2. List of 153 multiple systems detected visually (adaptive optics, lucky imaging, coronagraphy) and involving M dwarfs from our sample.

2MASS name	Common name	N (component)	Pair	ρ or a (arcsec)	θ (deg)	PM, orbit	Discovery
J00155808−1636578		2		0.1045	90		Shkolnik et al. (2012)
J00161455+1951385	GJ 1006A	3 (A)	AB	25.2	58		1936
			AC	9.6	336		1969
J00182256+4401222	Gl 15A	2 (A)	AB	34.3	64	CPM, OM	1860
J00182549+4401376	Gl 15B	2 (B)	AB	34.3	64	CPM, OM	1860
J00233468+2014282	FK Psc	2		1.6	143		Skiff (private communication) to WDS
J00340843+2523498	V493 And	2		1.5	103		Skiff (private communication) to WDS
J00424820+3532554	Gl 29.1A	2 (A)	AB	15.8	271		1950
			A			SB2	This work
J00485822+4435091	GJ 3058	2 (AB)	AB	1.027	256	CPM, OM	McCarthy, Zuckerman & Becklin (2001)
J01023895+6220422	Gl 49	2 (A)	AB	294.8	76		1952
J01031971+6221557	Gl 51	2 (B)	AB	294.8	76		1952
J01034013+4051288	G 132-50	4 (A)	AB	26.4	120	CPM	1960
			Aab	0.267	308		Shkolnik et al. (2012)
J01034210+4051158	G 132-51	4 (BC)	BC	2.477	97	CPM	1960
J01112542+1526214	GJ 3076	2		0.327	241	CPM, OM	Beuzit et al. (2004)
J01155017+4702023		4 (AB)	AB-CD	27.1	330	CPM?	1998
			AB	0.272	250		Law, Hodgkin & Mackay (2008)
			CD	0.271	268		Janson et al. (2012)
J01365516−0647379	G 271-110	2				CPM with EX Cet	Shkolnik et al. (2012)
J01373940+1835332	TYC 1208-468-1	2 (A)	AB	1.7	24		1968
J01390120−1757026	Gl 65	2 (AB)	AB	2.046	sma	OM	1935
J01451820+4632077	G 173-18	2				SB2, VB	Shkolnik et al. (2009, 2010)
J01535076−1459503		2	AB	2.879	292	CPM	Bergfors et al. (2010)
J01591239+0331092	GJ 1041A	3 (A)	AB	3.2	53		1960
J01591260+0331113	GJ 1041B	3 (Bab)	Bab			SB2	Shkolnik et al. (2009)
J02110221−3540146	HIP 10191	3 (A)	AB	3.4	143		1925
			AC	13.3	37		1912
J02132062+3648506		2		0.217	76	CPM, OM	Janson et al. (2012)
J02155892−0929121		4 (AabBC)	Aab	0.042	308		Bowler et al. (2015b)
			AB	0.576	290	CPM, OM	Bergfors et al. (2010)
			AC	3.43	299	CPM	Bergfors et al. (2010)
J02272804+3058405	BD+30 397B	2 (B)	AB	22.0	316		1954
J02272924+3058246	AG Tri	2 (A)	AB	22.0	316		1954
J03143273+5926160	G 246-29	2					This work
J03192872+6156045	G 246-33	2		0.384	241		Janson et al. (2014)
J03323578+2843554		3	AB	0.482	106	CPM	Janson et al. (2012)
			BC	0.098	282	CPM	Janson et al. (2012)
J03373331+1751145	GJ 3239	4 (Aab)	AB	16.2	151		1960
			Aab			SB2	Shkolnik et al. (2010)
			Bab			E?SB2	Shkolnik et al. (2010)
J03591438+8020019		2		0.200	357		Janson et al. (2012)
J04134585−0509049	G 160-54	4 (Aab)	AB	3.332	108		Bowler et al. (2015a)
			Aab	0.1667	123	SB3	Bowler et al. (2015a,b)
J04311147+5858375	Gl 169.1A	3 (Aab)	AB	9.88	60	CPM	1908
			Aab	0.07	sma	OM	Strand (1977)
J05024924+7352143		2		0.301	82	CPM	Janson et al. (2012)

Table A2 *– continued*

2MASS name	Common name	*N* (component)	Pair	ρ or a (arcsec)	θ (deg)	PM, orbit	Discovery
J05031607+2123563	HD 285190	4 (Aab)	AB	166.3	241		1960
			Aab			SB2	This work
			Bab	0.302	168	CPM	Law et al. (2008)
J05100427−2340407		4 (Aab)	A-BC	27.2	18		1998
			Aab	0.522	128	CPM, OM	Janson et al. (2012)
			BC	1.815	307	CPM	Janson et al. (2012)
J05241914−1601153		2		0.613	68	CPM, OM	Bergfors et al. (2010)
J06103462−2151521	Gl 229	2 (A)	AB	6.8	168		Nakajima et al. (1995)
J06211300+4414307	GJ 3391	2		1.319	204		Cortés-Contreras et al. (2017)
J07272450+0513329	Gl 273	2		0.17	327		Ward-Duong et al. (2015)
J07293108+3556003		2		0.198	262	CPM, OM	Janson et al. (2012)
J07313848+4557173		2		0.206	353	CPM, OM	Janson et al. (2012)
J07315735+3613477	Gl 277B	3 (B)	AB	38.04	353	CPM	1930
J07315773+3613102	Gl 277A	3 (A)	Aab	1.53	194	OM	Beuzit et al. (2004)
J07320291+1719103	G 88-36	3 (Aa or Ab ?)	Aab	5.1	116		*Hipparcos*
			AB	11.2	281		1960
J07343745+3152102	Gl 278C	6 (C)	AB	6.805	sma	CPM, OM, DESB2	1778
			Aab			SB1	Vinter Hansen (1940)
			Bab			SB1	Vinter Hansen (1940)
			AC	70.1	163	CPM	1822
			Cab			DESB2	Joy & Sanford (1926); van Gent (1926)
J07345632+1445544	TYC 777-141-1	2		1.00	293		Cortés-Contreras et al. (2017)
J07384089−2113276	LHS 1935	2					
J07505369+4428181		2		2.031	142	CPM	Janson et al. (2012)
J07583098+1530146	GJ 3468	2 (A)	AB	16.1	208		1960
J08081317+2106182	GJ 3481	4 (A)	AB	10.633	144	CPM	1893
			Bab			SB2	Shkolnik et al. (2010)
			BabC	0.580	36		Shkolnik et al. (2010)
J08085639+3249118	GJ 1108A	4 (Aab)	AB	13.9	240		1950
			Aab	0.25			Brandt et al. (2014)
			Bab			SB2	Shkolnik et al. (2010)
J08103429−1348514	Gl 297.2B	3 (Bab)	AB	97.3	236	CPM	1920
			Bab	0.913	283		Jódar et al. (2013)
J08310177+4012115		2		1.899	122	CPM	Mason et al. (2001)
J08313744+1923494	GJ 2069B	5 (Bab)	Bab (or BD)	0.957	191	SB2 not confirmed	Delfosse et al. (1999b), this work
J08313759+1923395	GJ 2069A	5 (AabE)	AB	9.7	349	CPM	1936
			Aab (or AC)	0.0028	sma	OM, DESB2	Delfosse et al. (1999b)
			AE	0.536	181		Beuzit et al. (2004)
J08524466+2230523	NLTT 20426	2		4.6			
J08585633+0828259	GJ 3522	3 (AC-B)	AC-B	0.424	sma	CPM, OM	Delfosse et al. (1999b)
			Aab (or AC)			SB2	Reid & Gizis (1997)
J09142298+5241125	Gl 338A	3 (Aab)	AB	16.725	sma	CPM, OM	1821
			Aab			SB1	Cortés-Contreras et al. (2017)
J09142485+5241118	Gl 338B	3 (B)	AB	16.725	sma	CPM, OM	1821
J09423493+7002024	Gl 360	2 (A)	AB	89	77	CPM	1894
J10141918+2104297	GJ 2079	2		0.095	320	SB1 ?	Makarov & Kaplan (2005)
J10193634+1952122	Gl 388	4 (Cab)	AB	4.7	127		1820
			AC	336.0	288		1851
			Cab	0.110	sma	OM	Reuyl (1943)
J10452148+3830422	Gl 400	2		1.791	sma	OM	Hartkopf et al. (1994)
J11052903+4331357	Gl 412A	2 (A)	AB	31.8	125	CPM	1950
J11053133+4331170	Gl 412B	2 (B)	AB	31.8	125	CPM	1950
J11110245+3026415	Gl 414B	2 (B)	AB	34.1	263	CPM	1844
J11115176+3332111	GJ 3647	2		5.1			
J11200526+6550470	Gl 424	2		0.132	334		Tamazian, Docobo & Balega (2008)
J11220530−2446393	TWA 4	4 (AB)	AB	1.030	sma		1909
			Aab			SB1	Torres et al. (1995)
			Bab	0.0233	sma	OM, SB2	Torres et al. (1995)
J11515681+0731262		3 (AabB)	AB	0.514	107		Bowler et al. (2015b)
			Aab			SB2	Bowler et al. (2015b)
J12290290+4143497	GJ 3729	2		0.0503	256	SB2	Shkolnik et al. (2012)
J12490273+6606366	Gl 487	3 (AabB)	AB	0.297	15		Delfosse et al. (1999b)
			AabB			SB3	Delfosse et al. (1999b)

Table A2 – *continued*

2MASS name	Common name	*N* (component)	Pair	ρ or a (arcsec)	θ (deg)	PM, orbit	Discovery
J12574030+3513306	Gl 490A	4 (Aab)	AB	16.0	227	CPM	1950
			Aab	0.10	240		Shkolnik et al. (2012)
J12573935+3513194	Gl 490B	4 (Bab)	Bab	0.20	310		Shkolnik et al. (2012)
J13004666+1222325	Gl 494	3 (AB)	AB	0.051	sma	OM	Heintz (1994); Beuzit et al. (2004)
			AC	102.1	220	CPM	Goldman et al. (2010)
J13093495+2859065	GJ 1167A	2		193.6	28	CPM	1965
J13142039+1320011	NLTT 33370	2		0.2	50		Law, Hodgkin & Mackay (2006)
J13282106−0221365	Gl 512A	2 (A)	AB	8.5	52	CPM	1937
J13314666+2916368	GJ 3789	2 (AB)	AB	0.190	85		Beuzit et al. (2004)
J13345147+3746195		2		0.082	198		Daemgen et al. (2007)
J13414631+5815197		2		0.699	251	CPM, OM	Janson et al. (2012)
J14154197+5927274		2		5.064	231		Cortés-Contreras et al. (2017)
J14170294+3142472	GJ 3839	2		0.439	219	SB3	Delfosse et al. (1999b), Forveille (private communication)
J14493338−2606205	Gl 563.2A	3 (Aab)	AB	26.7	244		1920
			Aab			SB2	This work
J14511044+3106406	G 166-49	2		2.353	48	CPM, OM	Janson et al. (2012)
			Aab			SB2	This work
J15123818+4543464	GJ 3898	2		0.481	220		McCarthy et al. (2001)
J15235385+5609320		2	AB	68	248		1912
			A			SB2	This work
J15493833+3448555	GJ 3919	2		0.208	99		Cortés-Contreras et al. (2017)
J15553178+3512028	GJ 3928	2		1.620	255		McCarthy et al. (2001)
J15594729+4403595		2		5.67	284	CPM?	2000
J16164537+6715224	Gl 617B	2 (B)	AB	64.5	13		1892
J16170537+5516094	Gl 616.2	2		0.148	sma	SB2, OM	Shkolnik et al. (2010)
J16240913+4821112	Gl 623	3 (Aab)	AB	176	288		1911
			Aab	0.2397	sma	OM, SB1	Martinache et al. (2007)
J16352740+3500577	GJ 3966	2		0.0922	26		Bowler et al. (2015a)
J16411543+5344110		2		0.099	94	CPM, OM, SB2?	Janson et al. (2012), this work
J16552880−0820103	Gl 644	5 (AB)	AB	0.2256	sma	OM	1934
			Bab			SB2 (3?)	Pettersen et al. (1984)
			AB-C	72.2	313	CPM	1920
J16553529−0823401	Gl 644C	5 (F)	AB-F	230.6	155	CPM	1954
J16575357+4722016	Gl 649.1B	3 (B)	AB	2.79	sma	OM	1908
			AC	89.1	sma	OM	1823
J16590962+2058160	V1234 Her	2		0.689	139	CPM, OM	Janson et al. (2012)
J17021204+5103284		2		0.816	63	CPM	Janson et al. (2012)
J17035188+3211523	LP 331-57B	2 (B)	AB	1.260	143	CPM, OM	Daemgen et al. (2007)
J17035283+3211456	LP 331-57A	2 (A)	AB	1.260	143	CPM, OM, SB2?	Daemgen et al. (2007), this work
J17155010+1900000	GJ 3997	2		1.841	267		Jódar et al. (2013)
J17195422+2630030	Gl 669A	3 (A)	AB	16.7	269	CPM	1936
			Bab				Shkolnik et al. (2012)
J17294104−1748323	BD-17 4821B	2 (B)	AB	8.5	194		1830
J17362594+6820220	Gl 687	4 (Bab)	AB	180.4	210		1877
			Aab	0.30	352		1984
			Bab	0.033	sma	OM	Lippincott (1977)
J17375330+1835295	Gl 686	2		0.040	sma	OM	Bieger Smith (1964)
J17380077+3329457		2		1.029	158	CPM?	Janson et al. (2012)
J17462507+2743014	Gl 695BC	5 (BC)	AD	321.1	5		1921
			A-BC	35.5	249	CPM	1781
			Aab	0.265	sma	OM	1998
			BC	1.36	sma	OM	1854
J18130657+2601519	GJ 4044	3		1.45	226	CPM	Shkolnik et al. (2012)
J18351833+4544379	Gl 720A	2 (A)	AB	112.1	56		1960
J18410977+2447143	GJ 1230A	3 (Aab)	AB	4.83	6		1905
			Aab			SB2	Gizis & Reid (1996)
J18424666+5937499	Gl 725A	3 (A)	AB	13.88	sma	CPM, OM	1831
J18424688+5937374	Gl 725B	3 (Bab)	Bab	0.028	sma	OM	Baize (1976)
J18440971+7129178		2	AB	2.30	97		1963
J18441019+7129175		2	AB	2.30	97		1963
J18561590+5431479	G 229-18	3 (Aab)	Aab	0.4	306	SB2	1991
			AB	118.8	170		1905

Table A2 – *continued*

2MASS name	Common name	*N* (component)	Pair	ρ or a (arcsec)	θ (deg)	PM, orbit	Discovery
J19071320+2052372	Gl 745B	2 (A)	AB	114.5	290	CPM	1897
J19165762+0509021	Gl 752B	2		75.8	152	CPM	1942
J19445376−2337591	LP 869-26	2 (AB)	AB	0.60	341		Montagnier et al. (2006)
J19535443+4424541	GJ 1245A	3 (Aab)	Aab	0.8267	sma	OM	Harrington & Dahn (1984)
J19535508+4424550	GJ 1245B	3 (B)	AB	6.454	70		1954
J20163382−0711456	TYC 5174-242-1	2		0.107	352	CPM?	Janson et al. (2012)
J20294834+0941202	Gl 791.2	2 (AB)	AB	0.1037	sma	OM	Benedict et al. (2000)
J20434114−2433534		2		1.48			Shkolnik et al. (2012)
J20450949−3120266	Gl 803	3 (A)	A-BC		213		1920
			BC	3.18	sma	OM	1913
J20531465−0221218	LP 636-19	2	AB	0.086	321		Janson et al. (2012)
J21000529+4004136	Gl 815	3 (AB)	AB	0.685	39		1934
			Aab			SB2	Karataş et al. (2004)
J21374019+0137137	2E 4498	2		0.433	341		Janson et al. (2014)
J21514831+1336154	GJ 4228	2		0.674	131		Cortés-Contreras et al. (2017)
J22143835−2141535	BD-22 5866	4		0.104		ESB4	Shkolnik et al. (2008)
J22171870−0848186	Gl 852B	3 (Bab)	AB	7.954	213	CPM	1920
			Bab	0.970	317	CPM, OM	Beuzit et al. (2004)
J22171899−0848122	Gl 852A	3 (A)	AB	7.954	213	CPM	1920
J22232904+3227334	Gl 856	2	AB	1.61	sma	CPM, OM	1959
J22384530−2036519	Gl 867B	4 (B)	AC-BD	24.5	350	CPM	1830
			Bab (or BD)			SB1	Davison et al. (2014)
J22384559−2037160	Gl 867A	4 (A)	Aab (or AC)			SB2	Herbig & Moorhead (1965)
J22450004−3315258	Gl 871.1B	2	AB	35.8	133	CPM	1920
J22465311−0707272	UCAC4 415-145732	2					
J22554384−3022392	LP 933-24	2 (A)	AB	5.8	163	CPM	1960
J23062378+1236269	G 67-46	3 (Aab)	AB	37.3	36	CPM	1951
			Aab	0.426	317	CPM, OM, SB2 (3?)	Shkolnik et al. (2010)
J23172441+3812419	GJ 4327	3 (Bab)	AB	18.1	253		1929
			Bab			SB2	Cortés-Contreras et al. (2017)
J23172807+1936469	GJ 4326	2	AB	0.264	sma	CPM, OM	Beuzit et al. (2004)
J23205766−0147373	LP 642-48	2	AB	0.099	325		Daemgen et al. (2007)
J23292258+4127522	GJ 4338B	3 (Bab)	AB	17.7	214		1952
			Bab	0.257	209		Shkolnik et al. (2012)
J23292346+4128068	GJ 4337A	3 (A)	AB	17.7	214		1952
J23315208+1956142	Gl 896A	2 (A)	AB	7.6	sma	CPM	1941
J23315244+1956138	Gl 896B	2 (B)	AB	7.6	sma	CPM	1941
J23495365+2427493		2		0.131	325	CPM, OM	Janson et al. (2012)
J23513366+3127229		2 (A)	AB	2.386	92	CPM	Bowler et al. (2012)
J23574989+3837468	GJ 4381	2	AB	0.50	247		McCarthy et al. (2001)
J23581366−1724338	LP 764-40	2	AB	1.989	356	CPM, OM	Daemgen et al. (2007)
J23584342+4643452	Gl 913	2		0.0341	sma	OM,SB2?	Goldin & Makarov (2007)

A3 Comparison of effective temperatures and metallicities between the present work and a reference (Mann et al. 2015)

Table A3 gives a comparison between our results for $T_{\rm eff}$ and [Fe/H] using the MCAL method, with state of the art reference values taken from Mann et al. (2015).

A4 Comparison of equatorial and projected rotation velocities

Table A4 gives the comparison of equatorial rotation velocities computed from photometric rotation periods and radii, with projected rotation velocities for the slow rotators.

Table A5 gives the same comparison for the resolved rotators ($v_{\rm eq} > 3\,{\rm km\,s^{-1}}$). For LP 193-584, the rotation period from Hartman et al. (2011) is uncertain and therefore given in parentheses, as well as the affected value of $v_{\rm eq}$. For NLTT 3478, the very large difference between $v_{\rm eq}$ and $v\sin i$ would imply an improbable small value of the inclination. The photometric period should therefore be measured again.

A5 Master table of properties for the stars in our sample

A summary of the measurements for the whole sample of 440 stars is given in Table A6, an extract of which ($0 < {\rm RA} < 2\,{\rm h}$) is given here. There are actually 447 entries, as observations for some stars in the initial sample but later rejected are listed, and some close binaries appear with two different entries, one for each component. For each star are listed the number of observed spectra, including those finally rejected for the measurement of metallicity and effective temperature, the spectroscopic mode of observation (polarimetric or S+S), the spectral type from the TiO_5 index, the $V-K_s$ colour, the H magnitude from the 2MASS PSC, the HRV averaged over all spectra for the star (not given for SB2), the projected rotational velocity and its error (or $<2\,{\rm km\,s^{-1}}$ when unresolved), the Hα

Table A3. List of 74 stars with measurements of $T_{\rm eff}$ and [Fe/H] in Mann et al. (2015, called reference) compared to our measurements (called this work) when they exist (66 stars, SB1 and SB2 rejected). Stars with an * after the common name are the 29 used to recalibrate the MCAL method. Active stars have values in parentheses.

2MASS name	Common name	$T_{\rm eff}$ (this work)	$T_{\rm eff}$ (reference)	[Fe/H] (this work)	[Fe/H] (reference)
J00115302+2259047	LP 348-40	3372	3359	+0.13	+0.13
J00182256+4401222	Gl 15A	3562	3603	−0.33	−0.30
J00182549+4401376	Gl 15B	3402	3218	−0.44	−0.30
J01123052−1659570	Gl 54.1*	(3344)	3056	(−0.34)	−0.26
J01432015+0419172	Gl 70	3482	3458	−0.10	−0.13
J02122090+0334310	Gl 87*		3638		−0.36
J02190228+2352550	GJ 3150	(3058)	3216	(−0.35)	−0.07
J02221463+4752481	Gl 96	4001	3785	+0.34	+0.14
J02333717+2455392	Gl 102	(3152)	3199	(−0.31)	0.00
J02361535+0652191	Gl 105B*		3284		−0.12
J02441537+2531249	Gl 109	3423	3405	−0.10	−0.10
J04374092+5253372	Gl 172	3824	3929	+0.36	−0.11
J04374188−1102198	Gl 173	3747	3671	−0.02	−0.04
J04425581+1857285	Gl 176*		3680		+0.14
J05015746−0656459	LHS 1723	3519	3143	−0.38	−0.06
J05032009−1722245	LP 776-46	3398	3365	−0.21	−0.12
J05312734−0340356	Gl 205*	3964	3801	+0.53	+0.49
J05363099+1119401	Gl 208	3937	3966	+0.52	+0.05
J05420897+1229252	Gl 213*	3253	3250	−0.19	−0.22
J06000351+0242236	GJ 3379	(2488)	3214	(−0.14)	+0.07
J06011106+5935508	GJ 3378	3241	3340	−0.06	−0.09
J06521804−0511241	Gl 250B*		3481		+0.14
J06544902+3316058	Gl 251	3415	3448	−0.03	−0.02
J07272450+0513329	Gl 273*	3323	3317	−0.06	−0.11
J07284541−0317524	GJ 1097	3423	3448	−0.07	−0.01
J07384089−2113276	LHS 1935	3446	3358	−0.21	−0.18
J08103429−1348514	Gl 297.2B	3912	3544	+0.15	0.00
J08160798+0118091	GJ 2066*	3571	3500	−0.10	−0.12
J09142298+5241125	Gl 338A	3920	3920	+0.37	−0.01
J10112218+4927153	Gl 380	4172	4131	+0.83	+0.24
J10121768−0344441	Gl 382*	3694	3623	+0.16	+0.13
J10285555+0050275	Gl 393*	3576	3548	−0.13	−0.18
J10505201+0648292	Gl 402	3216	3238	−0.03	+0.16
J11032023+3558117	Gl 411	3561	3563	−0.44	−0.38
J11052903+4331357	Gl 412A	3552	3619	−0.40	−0.37
J11414471+4245072	GJ 1148	3236	3304	+0.09	+0.07
J11421096+2642251	Gl 436*	3500	3479	+0.01	+0.01
J11474440+0048164	Gl 447*	3244	3192	−0.14	−0.02
J11505787+4822395	GJ 1151	3304	3118	−0.14	+0.03
J12100559−1504156	GJ 3707	3161	3385	+0.19	+0.26
J12385241+1141461	Gl 480	3384	3463	+0.22	+0.26
J13282106−0221365	Gl 512A	3433	3498	+0.11	+0.08
J13295979+1022376	Gl 514*	3747	3727	−0.01	−0.09
J13454354+1453317	Gl 526*	3698	3649	−0.31	−0.31
J14341683−1231106	Gl 555*	3211	3211	+0.11	+0.17
J15192689−0743200	Gl 581*	3401	3395	−0.14	−0.15
J16252459+5418148	Gl 625	3557	3475	−0.40	−0.35
J16301808−1239434	Gl 628*	3327	3272	−0.03	−0.03
J16570570−0420559	GJ 1207	(1624)	3229	(−0.14)	−0.09
J17302272+0532547	Gl 678.1A*		3675		−0.09
J17362594+6820220	Gl 687	3424	3439	−0.03	+0.05
J17375330+1835295	Gl 686*	3693	3657	−0.21	−0.25
J17435595+4322441	Gl 694	3557	3464	+0.05	0.00
J17575096+4635182	GJ 4040	3393	3470	+0.04	+0.04
J18050755−0301523	Gl 701*		3614		−0.22
J18415908+3149498	GJ 4070	3473	3400	−0.17	−0.16
J18424666+5937499	Gl 725A	3470	3441	−0.32	−0.23
J18424688+5937374	Gl 725B	3300	3345	−0.30	−0.30
J19071320+2052372	Gl 745B	3495	3494	−0.44	−0.35
J19165526+0510086	Gl 752A*		3558		+0.10
J20450403+4429562	Gl 806	3748	3542	−0.14	−0.15

Table A3 *– continued*

2MASS name	Common name	$T_{\rm eff}$ (this work)	$T_{\rm eff}$ (reference)	[Fe/H] (this work)	[Fe/H] (reference)
J20523304−1658289	LP 816-60	3196	3205	−0.05	−0.02
J20564659−1026534	Gl 811.1	3512	3473	+0.10	+0.16
J21091740−1318080	Gl 821	3633	3545	−0.65	−0.45
J22021026+0124006	Gl 846*	3879	3848	+0.27	+0.02
J22094029−0438267	Gl 849*	3490	3530	+0.22	+0.37
J22531672−1415489	Gl 876*	3166	3247	+0.12	+0.17
J23213752+1717284	GJ 4333	3153	3324	+0.19	+0.24
J22563497+1633130	Gl 880*	3887	3720	+0.27	+0.21
J23055131−3551130	Gl 887*		3688		−0.06
J23415498+4410407	Gl 905	3186	2930	−0.10	+0.23
J23430628+3632132	GJ 1289	(3193)	3173	(−0.08)	+0.05
J23491255+0224037	Gl 908*	3602	3646	−0.52	−0.45

index (above 0.25, $T_{\rm eff}$ and [Fe/H] cannot be reliably measured by the MCAL method), our mean value of [Fe/H] and $T_{\rm eff}$ for the inactive stars (Hα index <0.25), the predicted uncertainty of the RV assuming a full correction of telluric lines (see Section 6), and a binarity flag (SB1 for a single-line spectroscopic binary, SB2 for a multiple-lines spectroscopic binary, and VB for a visual binary with a projected separation smaller than 2.0 arcsec). The uncertainties on $T_{\rm eff}$ and [Fe/H] are computed from the individual internal uncertainties returned by the MCAL method. They do not reflect systematic uncertainties associated with this method. Our measurements of $T_{\rm eff}$ and [Fe/H] are given the source code 1. When they are not available, we used the values listed in Mann et al. (2015) with a source code 2, or values without error derived using their equation (7) and coefficients in Table 2 with a source code 3. The full table is available online. The first page is displayed here to illustrate the format.

Table A4. List of 54 slow rotators with a time-series measurement of the rotation period (in days), together with their adopted radius in $\mathcal{R}_{\odot}^{N}$ and derived v_{eq} in $\mathrm{km\,s^{-1}}$, to be compared to our measure or upper limit of $v\sin i$ in $\mathrm{km\,s^{-1}}$.

2MASS name	Common name	P_{rot}	Reference	Radius	v_{eq}	$v\sin i$
J00161455+1951385	GJ 1006A	4.798	Newton et al. (2016)	0.24	2.58	4.0 ± 1.6
J00240376+2626299		29.84	Newton et al. (2016)	0.21	0.36	2.6 ± 1.0
J01023895+6220422	Gl 49	18.6	Donati et al. (2008)	0.46	1.26	<2
J01123052−1659570	Gl 54.1	69.2 ± 0.1	Suárez Mascareño, Rebolo & González Hernández (2016)	0.18	0.13	3.4 ± 0.8
J04274130+5935167	GJ 3287	6.850	Newton et al. (2016)	0.22	1.62	3.9 ± 1.5
J05015746−0656459	LHS 1723	88.5	Kiraga (2012)	0.21	0.12	3.8 ± 1.3
J05312734−0340356	Gl 205	35.0 ± 0.1	Suárez Mascareño et al. (2015)	0.62	0.89	<2
J05335981−0221325		7.25	Kiraga (2012)	0.32	2.23	5.4 ± 1.0
J05363099+1119401	Gl 208	12.04	Kiraga (2012)	0.70	2.95	4.0 ± 1.4
J06103462−2151521	Gl 229	27.3 ± 0.1	Suárez Mascareño et al. (2016)	0.57	1.05	<2
J07320291+1719103	G 88-36	13.41	Hartman et al. (2011)	0.72	2.73	3.0 ± 1.6
J09360161−2139371	Gl 357	74.30 ± 1.70	Suárez Mascareño et al. (2015)	0.39	0.26	2.5 ± 1.1
J09562699+2239015	LHS 2212	107.8	Newton et al. (2016)	0.21	0.097	<2
J10121768−0344441	Gl 382	21.56	Kiraga (2012)	0.45	1.17	<2
J11023832+2158017	Gl 410	14.0	Donati et al. (2008)	0.58	2.10	3.0 ± 0.7
J11032023+3558117	Gl 411	48.00	Kiraga & Stepien (2007)	0.48	0.51	<2
J11032125+1337571	NLTT 26114	34.42	Newton et al. (2016)	0.25	0.37	4.6 ± 1.6
J11115176+3332111	GJ 3647	7.785	Newton et al. (2016)	0.28	1.83	4.6 ± 0.7
J11200526+6550470	Gl 424	149.7	Engle, Guinan & Mizusawa (2009)	0.61	0.20	<2
J11414471+4245072	GJ 1148	73.498679	Hartman et al. (2011)	0.24	0.16	<2
J11421096+2642251	Gl 436	39.90 ± 0.80	Suárez Mascareño et al. (2015)	0.35	0.45	<2
J11474440+0048164	Gl 447	165.1 ± 0.8	Suárez Mascareño et al. (2016)	0.20	0.063	2.1 ± 1.0
J11505787+4822395	GJ 1151	132	Irwin et al. (2011)	0.19	0.072	2.5 ± 1.0
J13101268+4745190	LHS 2686	28.80	Newton et al. (2016)	0.17	0.29	4.5 ± 0.9
J13295979+1022376	Gl 514	28.0 ± 2.9	Suárez Mascareño et al. (2015)	0.54	0.98	2.0 ± 0.8
J13454354+1453317	Gl 526	52.3 ± 1.7	Suárez Mascareño et al. (2015)	0.50	0.48	<2
J14010324−0239180	Gl 536	43.3 ± 0.1	Suárez Mascareño et al. (2016)	0.53	0.62	<2
J15192689−0743200	Gl 581	130.00 ± 2.00	Robertson et al. (2014)	0.32	0.12	<2
J15323737+4653048	TYC 3483-856-1	10.585	Hartman et al. (2011)	0.49	2.35	3.4 ± 1.6
J15553178+3512028	GJ 3928	3.542	Newton et al. (2016)	0.19	2.71	6.9 ± 0.8
J15581883+3524236	G 180-18	57.216476	Hartman et al. (2011)	0.29	0.26	<2
J16252459+5418148	Gl 625	77.8 ± 5.5	Suárez Mascareño et al. (2017)	0.42	0.28	2.2 ± 0.7
J16301808−1239434	Gl 628	119.3 ± 0.5	Suárez Mascareño et al. (2016)	0.26	0.11	<2
J16360563+0848491	GJ 1204	6.331	Newton et al. (2016)	0.22	1.80	3.0 ± 0.7
J17195422+2630030	Gl 669A	20.263417	Hartman et al. (2011)	0.27	0.68	3.2 ± 0.7
J17574849+0441405	Gl 699	130	Kiraga & Stepien (2007)	0.24	0.095	3.1 ± 1.2
J17575096+4635182	GJ 4040	31.643331	Hartman et al. (2011)	0.31	0.50	2.0 ± 1.1
J18073292−1557464	GJ 1224	<4.3	Morin et al. (2010)	0.18	>2.0	4.3 ± 0.7
J18172513+4822024	TYC 3529-1437-1	16.2578	Norton et al. (2007)	0.38	1.19	3.1 ± 1.0
J18424498+1354168	GJ 4071	8.090	Newton et al. (2016)	0.22	1.41	4.2 ± 0.7
J18441139+4814118		21.522016	Hartman et al. (2011)	0.32	0.75	2.7 ± 1.0
J20414744+4938482		104.50	Newton et al. (2016)	0.22	0.11	<2
J20523304−1658289	LP 816-60	67.6 ± 0.1	Suárez Mascareño et al. (2016)	0.22	0.17	<2
J22004701+7949254	NLTT 52801	75.41	Newton et al. (2016)	0.30	0.20	<2
J22094029−0438267	Gl 849	39.2 ± 6.3	Suárez Mascareño et al. (2015)	0.32	0.42	<2
J22245593+5200190	GJ 1268	81.77	Newton et al. (2016)	0.18	0.11	3.6 ± 1.0
J22250174+3540079		22.897888	Hartman et al. (2011)	0.39	0.86	2.3 ± 1.0
J22270871+7751579	G 242-2	98.42	Newton et al. (2016)	0.16	0.08	2.2 ± 1.0
J22523963+7504190	NLTT 55174	107.3	Newton et al. (2016)	0.18	0.087	<2
J22531672−1415489	Gl 876	95 ± 1	Nelson et al. (2016)	0.25	0.13	<2
J22563497+1633130	Gl 880	37.5 ± 0.1	Suárez Mascareño et al. (2015)	0.46	0.62	<2
J23380819−1614100	GJ 4352	61.66	Watson (2006)	0.42	0.34	2.1 ± 1.2
J23415498+4410407	Gl 905	99.58	Newton et al. (2016)	0.14	0.07	<2
J23545147+3831363		4.755	Newton et al. (2016)	0.25	2.64	5.4 ± 1.3

Table A5. List of 93 resolved rotators with a time-series measurement of the rotation period (in days), together with their adopted radius in $\mathcal{R}_{\odot}^{N}$ and derived v_{eq} in km s^{-1}, to be compared to our measure of $v\sin i$ in km s^{-1}.

2MASS name	Common name	P_{rot}	Reference	Radius	v_{eq}	$v\sin i$
J00233468+2014282	FK Psc	7.9165	Norton et al. (2007)	0.77	4.91	3.2 ± 0.7
J00243478+3002295	GJ 3033	1.0769	West et al. (2015)	0.19	8.88	12.2 ± 0.8
J00340843+2523498	V493 And	3.1555	Norton et al. (2007)	0.83	13.3	11.3 ± 1.9
J00485822+4435091	LP 193-584	(1.305)	Hartman et al. (2011)	0.30	(11.5)	15.6 ± 1.4
J01031971+6221557	Gl 51	1.0237	West et al. (2015)	0.19	9.34	12.5 ± 0.7
J01034013+4051288	NLTT 3478	0.253982	Hartman et al. (2011)	0.86	172	5.4 ± 1.1
J01220441−3337036		9.58	Kiraga (2012)	0.76	4.04	4.1 ± 1.1
J01362619+4043443	V539 And	0.4357	Norton et al. (2007)	0.42	48.2	73.2 ± 1.0
J01373940+1835332	TYC 1208-468-1	2.803	Kiraga (2012)	0.56	10.0	16.3 ± 1.4
J01390120−1757026	Gl 65A	0.2430 ± 0.0005	Barnes et al. (2017)	0.14	29.8	29.5 ± 0.7
J01390120−1757026	Gl 65B	0.2268 ± 0.0003	Barnes et al. (2017)	0.15	33.2	37.9 ± 1.4
J01535076−1459503		1.515	Kiraga (2012)	0.28	9.22	11.6 ± 1.7
J02001277−0840516		2.28	Kiraga (2012)	0.36	8.08	12.2 ± 2.1
J02071032+6417114	GJ 3134	1.177	Newton et al. (2016)	0.20	8.68	11.4 ± 1.0
J02155892−0929121		1.4374	Kiraga & Stępień (2013)	0.34	11.8	15.7 ± 1.3
J02272924+3058246	AG Tri	13.6928	Norton et al. (2007)	0.98	3.61	4.9 ± 2.0
J02364412+2240265	G 36-26	0.3697	West et al. (2015)	0.15	21.1	11.2 ± 1.4
J03153783+3724143	LP 247-13	1.2887	Hartman et al. (2011)	0.31	12.2	15.1 ± 0.9
J03472333−0158195	G 80-21	3.881	Kiraga (2012)	0.34	4.46	6.2 ± 1.1
J04302527+3951000	Gl 170	0.7177	West et al. (2015)	0.18	12.7	13.6 ± 0.8
J04353618−2527347	LP 834-32	2.785	Kiraga (2012)	0.26	4.70	7.1 ± 1.0
J04365738−1613065		0.6105	Kiraga (2012)	0.27	22.5	63.3 ± 8.4
J04435686+3723033	V962 Per	4.2878	Norton et al. (2007)	0.38	4.46	10.1 ± 1.6
J04571728−0621564		0.7337	Kiraga (2012)	0.63	43.2	11.0 ± 1.8
J04593483+0147007	Gl 182	4.414	Kiraga (2012)	0.63	7.19	8.7 ± 1.6
J05024924+7352143		0.68204	Kiraga & Stępień (2013)	0.95	70.5	46.1 ± 3.8
J06000351+0242236	GJ 3379	1.8088	West et al. (2015)	0.22	6.29	5.9 ± 1.4
J06362522+4349473		1.5945715	Hartman et al. (2011)	0.28	8.95	19.6 ± 1.0
J07310129+4600266		1.33064	Hartman et al. (2011)	0.23	8.82	14.9 ± 0.7
J07444018+0333089	Gl 285	2.7758 ± 0.0006	Morin et al. (2008b)	0.22	4.05	6.6 ± 0.8
J08085639+3249118	GJ 1108A	3.37045	Hartman et al. (2011)	0.65	9.80	9.5 ± 1.6
J08294949+2646348	GJ 1111	0.459	Newton et al. (2016)	0.19	20.7	11.4 ± 0.7
J09002359+2150054	LHS 2090	0.439	Newton et al. (2016)	0.12	14.2	15.0 ± 1.0
J09445422−1220544	G 161-71	0.4417	Kiraga (2012)	0.15	17.4	41.8 ± 5.0
J10141918+2104297	GJ 2079	7.861	Kiraga (2012)	0.60	3.87	5.5 ± 1.6
J10193634+1952122	Gl 388	2.2399 ± 0.0006	Morin et al. (2008b)	0.29	6.48	4.1 ± 0.7
J10481258−1120082	GJ 3622	1.5 ± 0.2	Morin et al. (2010)	0.13	4.42	3.3 ± 0.7
J10562886+0700527	Gl 406	<2.0	Morin et al. (2010)	0.12	>3.1	2.9 ± 0.8
J11015191−3442170	TW Hya	3.5683 ± 0.0002	Huélamo et al. (2008)	0.69	9.79	5.4 ± 0.7
J11053133+4331170	Gl 412B	0.78 ± 0.02	Morin et al. (2010)	0.13	8.56	8.0 ± 0.7
J11314655−4102473	Gl 431	0.9328	Kiraga (2012)	0.18	9.71	20.3 ± 0.8
J11324124−2651559	TWA 8A	4.638	Kiraga (2012)	0.30	3.32	5.1 ± 1.1
J11432359+2518137	GJ 3682	1.326	Newton et al. (2016)	0.23	8.78	13.7 ± 0.9
J12141654+0037263	GJ 1154	1.5835	West et al. (2015)	0.16	4.95	6.1 ± 0.7
J12185939+1107338	GJ 1156	0.491	Irwin et al. (2011)	0.14	14.9	15.6 ± 0.8
J12574030+3513306	Gl 490A	3.3664	Norton et al. (2007)	0.55	8.22	8.2 ± 1.6
J13003350+0541081	Gl 493.1	0.600	Irwin et al. (2011)	0.18	14.9	15.6 ± 0.8
J13004666+1222325	Gl 494	2.886	Kiraga (2012)	0.47	8.22	9.6 ± 0.9
J13093495+2859065	GJ 1167A	0.215	Newton et al. (2016)	0.20	47.3	51.3 ± 1.5
J13142039+1320011	NLTT 33370	0.158	Newton et al. (2016)	0.12	40.0	53.8 ± 1.6
J13314666+2916368	GJ 3789	0.2683	Norton et al. (2007)	0.22	42.0	76.0 ± 0.7
J13345147+3746195		3.0992	Hartman et al. (2011)	0.23	3.79	8.3 ± 0.8
J14142141−1521215	GJ 3831	0.2982	Kiraga (2012)	0.71	120	73.5 ± 0.7
J14200478+3903014	GJ 3842	0.3693	Norton et al. (2007)	0.34	46.2	70.0 ± 1.0
J14321078+1600494	GJ 3856	0.765	Newton et al. (2016)	0.23	15.5	14.1 ± 1.1
J14372948+4128350	LO Boo	2.09162	Hartman et al. (2011)	0.35	8.54	11.8 ± 1.2

Table A5 – *continued*

2MASS name	Common name	P_{rot}	Reference	Radius	v_{eq}	$v\sin i$
J15040626+4858538		1.02136	Hartman et al. (2011)	0.23	11.4	11.3 ± 2.0
J15123818+4543464	GJ 3898	1.686	Newton et al. (2016)	0.23	6.99	10.4 ± 1.1
J15215291+2058394	GJ 9520	3.3829	Norton et al. (2007)	0.42	6.22	5.2 ± 1.0
J15565823+3738137		0.30694	Hartman et al. (2011)	0.34	55.7	26.5 ± 1.4
J16352740+3500577	GJ 3966	0.9166	Norton et al. (2007)	0.24	13.0	21.5 ± 3.5
J16400599+0042188	GJ 3967	0.3114	West et al. (2015)	0.20	32.7	31.0 ± 0.8
J16402068+6736046	GJ 3971	0.3782	West et al. (2015)	0.13	17.5	10.8 ± 0.7
J16553529−0823401	Gl 644C	<1.0	Morin et al. (2010)	0.13	>6.5	10.1 ± 0.8
J16570570−0420559	GJ 1207	1.212	Kiraga (2012)	0.39	16.4	11.5 ± 1.5
J16590962+2058160	V1234 Her	4.1037	Norton et al. (2007)	0.27	3.32	6.5 ± 1.0
J17365925+4859460	V1279 Her	2.613578	Hartman et al. (2011)	0.36	6.91	7.0 ± 1.0
J17380077+3329457		12.184	Hartman et al. (2011)	0.80	3.30	7.2 ± 2.7
J18021660+6415445	G 227-22	0.280	Newton et al. (2016)	0.18	32.7	13.2 ± 1.2
J18130657+2601519	GJ 4044	2.285	Newton et al. (2016)	0.23	5.14	7.5 ± 0.7
J18315610+7730367	LP 24-256	0.8607	West et al. (2015)			15.8 ± 0.7
J19165762+0509021	Gl 752B	<0.8	Morin et al. (2010)	0.13	>8.2	5.3 ± 0.9
J19510930+4628598	GJ 1243	0.59258	Hartman et al. (2011)	0.23	19.6	22.1 ± 0.9
J19535443+4424541	GJ 1245AC	0.263241	Hartman et al. (2011)	0.14	25.9	22.0 ± 0.8
J19535508+4424550	GJ 1245B	0.71 ± 0.01	Morin et al. (2010)	0.13	9.48	7.9 ± 0.7
J20294834+0941202	Gl 791.2	0.3085 ± 0.0005	Barnes et al. (2017)	0.18	29.5	35.3 ± 0.7
J20450949−3120266	Gl 803	4.852	Kiraga (2012)	0.51	5.32	8.5 ± 0.7
J20465795−0259320		3.644	Kiraga (2012)	0.65	9.01	9.0 ± 1.7
J20560274−1710538	TYC 6349-200-1	3.403	Kiraga (2012)			12.4 ± 0.8
J21100535−1919573		3.710	Kiraga & Stępień (2013)	0.38	5.14	8.3 ± 0.9
J21374019+0137137	2E 4498	0.213086	Kiraga (2012)	0.22	51.5	49.9 ± 0.9
J22004158+2715135	TYC 2211-1309-1	0.5235	Norton et al. (2007)	0.70	67.9	61.6 ± 4.2
J22011310+2818248	GJ 4247	0.445654 ± 0.000002	Morin et al. (2008a)	0.23	26.2	36.9 ± 0.7
J22232904+3227334	Gl 856	0.8539	West et al. (2015)	0.32	18.8	16.2 ± 0.6
J22464980+4420030	Gl 873	4.3715 ± 0.0006	Morin et al. (2008b)	0.26	3.03	5.9 ± 0.7
J22515348+3145153	Gl 875.1	1.6404	Norton et al. (2007)	0.31	9.53	13.2 ± 0.9
J23060482+6355339	GJ 9809	2.831	Kiraga & Stępień (2013)	0.57	10.1	7.0 ± 1.4
J23081954−1524354	Gl 890	0.4311	Kiraga (2012)	0.66	76.9	69.4 ± 0.7
J23315208+1956142	Gl 896A	1.0664	Norton et al. (2007)	0.29	13.6	14.5 ± 0.8
J23315244+1956138	Gl 896B	0.404 ± 0.004	Morin et al. (2008b)	0.17	21.0	25.4 ± 0.9
J23320018−3917368		3.492	Kiraga (2012)	0.28	4.06	6.0 ± 1.1
J23512227+2344207	G 68-46	3.211	Newton et al. (2016)	0.22	3.39	5.2 ± 0.9
J23581366−1724338	LP 764-40	0.434093	Kiraga (2012)	0.37	42.7	28.6 ± 1.1

Table A6. Master list of data for the whole sample (440 dwarfs and 447 entries): number N of measured spectra, number n of rejected ones if any, instrument mode (P for polarimetry and/or S for S+S), spectral type (from TiO_5 index), $V-K_s$ colour, H magnitude, HRV, projected rotational velocity, and error in km s^{-1} (<2 if not resolved), Hα index, [Fe/H] and error, effective temperature and error in K, source code, RV uncertainty, and binarity flag (SB1, SB2, close VB).

2MASS name	Common name	Alt name	N	n	P/S	ST	$V-K_s$ (mag)	H (mag)	HRV (km s^{-1})	$v\sin i$ (km s^{-1})	err (km s^{-1})	Hα index	[Fe/H] (dex)	err (dex)	$T_{\rm eff}$ (K)	err (K)	source	$\sigma(RV)$ (m s^{-1})	Binarity
J00080642+4757025			1		S	4.3	5.102	8.000	−76.06						3129		3		SB2
J00115302+2259047	LP 348-40		1		S	4.1	5.015	8.308	−45.29	<2		0.05	0.126	0.036	3372	59	1	4.8	
J00155808−1636578			1		S	4.6	5.275	8.191	19.33	19.1	1.5	0.57			3077		3	25.2	VB
J00161455+1951385	GJ 1006A	EZ Psc	1		S	−1.0	5.058	7.322	4.72	4.0	1.6	−0.02	1.540	0.052	3678	84	1	2.0	
J00182256+4401222	Gl 15A	GX And	4		P	1.4	4.116	4.476	11.73	2.6	0.7	0.04	−0.329	0.005	3562	8	1	0.1	
J00182549+4401376	Gl 15B	GQ And	3		P	4.0	5.112	6.191	11.17	2.3	0.8	0.05	−0.437	0.011	3402	18	1	0.7	
J00210932+4456560			1		S	3.8	4.972	8.967	3.16	14.3	1.4	0.58			3214		3	57.3	
J00233468+2014282	FK Psc		3		S	−0.3	3.505	7.498	−2.19	3.2	0.7	0.09-0.13	0.933	0.015	3757	25	1	2.3	VB
J00240376+2626299			2		S	4.6	5.436	9.592	20.31	2.6	1.0	0.19-0.20	0.003	0.041	3504	68	1	17.3	
J00243478+3002295	GJ 3033		7		SP	4.8	5.623	9.218	10.23	12.2	0.8	0.52-0.64			2995		3	63.5	
J00294322+0112384			2		P	1.0	3.967	8.536	−31.57	<2		0.03	−0.167	0.010	3682	17	1	6.2	
J00340843+2523498	V493 And		2		S	−0.5	3.436	7.830	−9.63	11.3	1.9	0.14			3866		3	19.8	VB
J00385879+3036583	Gl 26	Wolf 1056	2		P	2.7	4.394	6.864	−0.37	<2		0.04	−0.093	0.010	3526	15	1	1.3	
J00424820+3532554	Gl 29.1A	FF And	1		S	1.4	4.106	6.506	−59.14						3508		3		SB2
J00433851+7545152			3		S	4.4	5.218	9.674	2.85	4.8	0.8	0.39-0.42			3117		3	15.5	
J00485822+4435091	LP 193-584	GJ 3058	1		S	3.7	4.851	8.485	−13.88	15.6	1.4	0.48			3248		3	36.7	VB
J00570261+4505099	G 172-30		2		P	3.4	4.731	7.459	6.62	2.1	1.1	0.05	−0.089	0.010	3407	16	1	2.2	
J00582789−2751251	Gl 46		2		P	3.8	4.883	7.203	21.76	2.5	1.3	0.05	−0.018	0.013	3361	20	1	1.7	SB1
J01012006+6121560	Gl 47		2		P	2.3	4.323	6.710	7.58	2.7	1.2	0.04-0.05	−0.218	0.008	3529	13	1	1.1	
J01023213+7140475	Gl 48		2		P	3.4	4.595	5.699	1.56	<2		0.03-0.04	0.044	0.010	3502	17	1	0.4	
J01023895+6220422	Gl 49	HIP 4872	1		S	1.6	4.194	5.582	−6.05	<2		0.04	0.249	0.011	3750	18	1	0.4	
J01031971+6221557	Gl 51	V388 Cas	26	1	P	5.4	5.635	8.014	−5.76	12.5	0.7	0.73-1.25			3003		3	20.2	
J01034013+4051288	NLTT 3478	G 132-50	1		S	3.5	3.370	7.466	−10.82	5.4	1.1	0.41			3908		3	13.9	VB
J01034210+4051158	NLTT 3481	G 132-51	1		S	4.6	4.584	8.839	−11.06	9.2	1.8	0.73			3301		3	52.5	
J01112542+1526214	GJ 3076		2		S	5.6	6.222	8.512	3.18	18.1	2.2	0.70-0.71			2826		3	27.0	VB
J01123052−1659570	Gl 54.1	YZ Cet	3		SP	5.0	5.676	6.749	28.27	3.4	0.8	0.14-0.61			2953		3	0.8	
J01155017+4702023			5		S	4.7	5.537	9.574	10.01	7.1	0.9	0.49-0.56			3044		3	93.9	VB
J01220441−3337036			2		S	0.0	3.568	7.636	4.86	4.1	1.1	0.11	0.569	0.018	3764	29	1	2.6	
J01351393−0712517			3		S	4.5	5.348	8.387	7.48						3081		3		SB2
J01362619+4043443	V539 And		1		S	1.6	4.364	9.073	−7.83	73.2	1.0	0.23			3418		3	67.9	
J01365516−0647379	G 271-110		3		S	4.3	5.196	9.137	12.77	11.5	0.8	0.70-0.71			3112		3	64.0	
J01373940+1835332	TYC 1208-468-1		2		S	−1.0	3.868	6.861	0.50	16.3	1.4	0.12			3571		3	8.5	VB
J01390120−1757026A	Gl 65A	BL Cet	4		P	5.9	6.320	6.520	19.82	29.5	0.7	0.39-0.67			2810		3	4.1	
J01390120−1757026B	Gl 65B	UV Cet	8		P	5.7	6.200	6.680	22.01	37.9	1.4	0.68-1.11			2842		3	4.9	
J01432015+0419172	Gl 70		4		P	2.5	4.332	6.809	−25.94	<2		0.04-0.05	−0.095	0.007	3482	11	1	1.2	
J01434512−0602400			1		S	4.0	5.037	8.174	−13.72						3171		3		SB2
J01451820+4632077	LHS 6032	G 173-18	1		S	2.6	4.339	7.423	36.79						3415		3		SB2
J01515108+6426060	GJ 3117A		2		P	2.6	4.478	7.250	−12.79	2.2	1.2	0.04	0.089	0.010	3620	17	1	1.9	
J01535076−1459503			2		S	3.8	4.940	7.297	10.34	11.6	1.7	0.56-0.57			3213		3	11.8	
J01591239+0331092	GJ 1041A	NLTT 6637	2		S	0.6	3.878	7.221	−7.98	2.4	1.2	0.02	0.073	0.012	3821	19	1	1.7	
J01591260+0331113	NLTT 6638		1		S	3.2	5.351	7.384	4.21						3087		3		SB2
J01592349+5831162	Gl 82	V596 Cas	1		S	4.7	5.194	7.224	−9.79	13.4	2.0	0.55			3107		3	10.4	

This paper has been typeset from a TEX/LATEX file prepared by the author.